THE ISOTOPE EFFECT IN ASDEX

M. Bessenrodt-Weberpals, F. Wagner
and the ASDEX Team

IPP 3/189 January 1993

MAX-PLANCK-INSTITUT FÜR PLASMAPHYSIK

8046 GARCHING BEI MÜNCHEN

MAX-PLANCK-INSTITUT FÜR PLASMAPHYSIK

GARCHING BEI MÜNCHEN

THE ISOTOPE EFFECT IN ASDEX

M. Bessenrodt-Weberpals, F. Wagner
and the ASDEX Team

IPP 3/189 January 1993

with contributions from

ICRH Team, LH Team, NI Team, Pellet Team, PSI Group,
O. Gehre, L. Giannone, J. Hofmann, A. Kallenbach,
K. McCormick, V. Mertens, H.D. Murmann, F. Ryter,
B.D. Scott, G. Siller, F.X. Söldner, A. Stäbler,
K.H. Steuer, U. Stroth, N. Tsois*, H. Verbeek, H. Zohm

*N.R.C.N.S. Democritos, Athens, Greece

Die nachstehende Arbeit wurde im Rahmen des Vertrages zwischen dem Max-Planck-Institut für Plasmaphysik und der Europäischen Atomgemeinschaft über die Zusammenarbeit auf dem Gebiete der Plasmaphysik durchgeführt.

Abstract — This paper describes the effect of the isotopic mass on plasma parameters as observed in the ASDEX tokamak. The paper comprises Ohmic as well as L-mode, H-mode and H*-mode scenarios. The measurements reveal that the ion mass is a substantial and robust parameter which affects all confinement times (energy, particle and momentum) in the whole operational window. Both, *core* properties like the sawtooth repetition time and *edge* properties like the separatrix density change with the isotopic mass. Specific emphasis is given to the edge parameters and changes of the edge plasma due to different wall conditioning such as carbonization and boronization. The pronounced isotope dependence of edge and divertor parameters are explained by the secondary effect of different power fluxes into the scrape-off layer plasma and onto the divertor plates. Finally, the observations serve to test different transport theories. With respect to the ion temperature gradient driven turbulence, the isotope effect is also studied in pellet refuelled discharges with peaked density profiles. The results from ASDEX are compared with those from other experiments.

PACS numbers : 52.50, 52.55, 52.70.

Contents

1 Introduction

The isotope effect was observed in ASDEX from its first operation days [1] till shutdown in 1990. During this time, there were various operational regimes where the hydrogen isotopes give rise to highly different confinement behaviour. In fact, isotopic dependences on the background ion mass A_i were investigated in limiter as well as various divertor configurations which had different conductances between the main plasma and the divertor chamber. The isotope effects prevail with various wall conditioning such as carbonization or boronization. Ohmic discharges show pronounced improvements for deuterium compared with hydrogen from low-density conditions in Linear Ohmic Confinement (LOC) up to the highest densities in Saturated Ohmic Confinement (SOC). The isotope effect also appears in L-mode plasmas with neutral injection (NI), with ion cyclotron resonance heating (ICRH), and with lower hybrid (LH) heating. Moreover, the improved confinement of H-mode plasmas shows isotopic dependences. It is noteworthy that there are four good confinement regimes which have only been achieved by operation in deuterium: these are Improved Ohmic Confinement (IOC) [2], sawtooth-free Ohmic discharges [3], counter-NI, and the H*-mode. These observations indicate that the isotope effect appears both when the *ion* transport dominates as in SOC and when the *electron* transport dominates as in LOC or with LH. To sum up, the background ion mass is a substantial and robust parameter of the confinement in various heating and confinement regimes of ASDEX, where deuterium plasmas always surpass hydrogen plasmas in all respects: energy, particle and momentum confinement.

Besides confinement, the central electron temperature T_{e0} is highly enhanced in deuterium plasmas and the sawtooth period τ_{ST} is appreciably prolonged compared with hydrogen plasmas. In particular, sawtooth-free discharges are achieved in deuterium plasmas only. Another MHD aspect, which is affected by the isotope mass, is the ELM frequency in H-mode discharges. ELMs like sawteeth are much more frequent in hydrogen than in deuterium plasmas. In the edge plasma, the isotope effect may be even more prominent, namely in the separatrix density n_{es}. The relations weaken, however, with improved wall conditioning and seem to be a corollary of the enhanced impurity radiation caused by improved particle confinement of deuterium. The better particle confinement time gives additionally rise to lower neutral pressure and consequently reduced impurity retention within the divertor chamber. The lower anomalous particle diffusion coefficient in combination with less ELMs and sawtooth activity aggrevates the impurity dilution and radiation problem in deuterium H-modes. In summary, we observe on ASDEX a shortening of both the confinement and the relaxation times when we switch from deuterium to hydrogen.

Besides ASDEX, there are many other tokamaks where the isotope effect has occurred in a similar form. Some of the earliest empirical scalings of tokamak confinement already included the beneficial properties of deuterium: Hugill and Sheffield [4] extracted for Ohmically heated tokamaks the four-parameter fit

$$\tau_E \propto \overline{n}_e^{0.61} \times a^{1.57} \times B_t^{0.88} \times A_i^{0.65}$$

and Pfeiffer and Waltz [5] derived from an extended data base that

$$\tau_E \propto \overline{n}_e^{0.59} \times a^{1.59} \times A_i^{0.30}.$$

As a consequence, the Goldston L-mode scaling [6]

$$\tau_E \propto I_p \times P^{-0.5} \times a^{-0.37} \times R^{1.75} \times \kappa^{0.5} \times A_i^{0.5}$$

takes an adhoc ansatz with an $A_i^{0.5}$ in it; the same exponent has been assumed in the Kaye-Goldston scaling [7] and the Kaye scaling [8]. The ITER L-mode power scaling [9]

$$\tau_E^{\mathrm{ITER89-P}} \propto I_p^{0.85} \times P_{\mathrm{tot}}^{-0.5} \times a^{0.3} \times R^{1.2} \times \kappa^{0.5} \times \overline{n}_e^{0.1} \times A_i^{0.5}$$

was also selected with an inherent isotope scaling.

Despite its fundamental nature and wide-spread appearance, conventional transport theories usually fail in predicting the right isotope effect on transport and confinement. Neoclassical theory, ion pressure gradient driven turbulence models and resistive ballooning theories, for instance, predict a degradation of confinement from deuterium to hydrogen. Recently, collisional drift-wave turbulence models seem to catch the right trends [10].

The remainder of this paper is organized as follows.

Firstly, we give a synopsis of the isotope effect in *various heating scenarios*, i.e. in Ohmic heating (Section 2) and in additional heating L-mode scenarios with neutral injection, ion cyclotron waves or lower hybrid waves (Section 3).

Then, the appearance of the isotope effect in *improved confinement scenarios* is discussed in Section 4. This includes IOC as well as H-mode or H*-mode.

Special emphasis is put on instabilities like sawteeth and ELMs which show significant isotope signature; this is the topic of Section 5.

Finally, the isotope effect on *other experiments* is addressed in Section 6. We give data of limiter tokamaks such as TEXTOR and also of divertor tokamaks such as Doublet III-D, which we gained from a world-wide questionnaire about the isotope effect. Information from the stellarators Wendelstein VII-AS and ATF are also included.

From the above phenomenology, the following questions arise.

(1) The first question, which is treated in Section 7, is *at what phase* of the discharge initiation the isotope effect makes its appearance, i.e. whether the isotope effect is already present during the plasma build-up.

(2) Next, in Section 8, we look at the operational window of the isotope effect in terms of various dimensionless quantities like collisionality etc.

(3) The *additive* nature of the isotope effect, viz. the role of the average ion mass in confinement, is treated in Section 9.

(4) Section 10 sheds light on the question whether the isotopic mass dependences as observed in the *edge plasma* are origin or consequence of the isotope effect. Here, we also propose a simple analytical model in order to describe the isotope dependences in the boundary plasma. These results are confirmed by extensive regression analysis.

(5) The next question is whether the ion or the electron transport or both are influenced by the isotope mix. To this aim, we follow in Section 11 the particle confinement time, derived from SOL and bulk plasma physics, and in Section 12 the momentum confinement time. We strongly refer to the observations of the various heating scenarios given in Section 3.

(6) Closely related to this question, we ask whether the isotope effect depends on the mass (A_i) or specific mass (A_i/Z_i). This is the subject of Section 13, which presents the results from helium discharges.

(7) An open question is whether the isotope effect *intrinsically* enters the diffusivities or whether the ion mass changes the *onset* conditions of an additional instability; this is looked at in Section 14. As a candidat, the damping of ion temperature gradient (ITG) driven turbulence is studied because the radial density profiles in deuterium are generally more peaked than in hydrogen. Since pellet refuelling gives rise to highly peaked density profiles in both hydrogen and deuterium plasmas, transport was explored for hydrogen pellet injection into hydrogen plasmas compared with deuterium pellet injection into deuterium plasmas. Both cases have sufficiently peaked density profiles such that the critical threshold for ITG driven turbulence should not be exceeded.

(8) We proceed by analyzing the isotopic dependences of the core and edge fluctuations and determine the particle fluxes from edge fluctuation studies (Section 15).

(9) On the way to understanding or even explaining the isotope effect, Section 16 presents some theoretical attempts. Theories based on particle drifts call for a lower transport for hydrogen plasmas because they rely on the ion gyroradius as characteristic length. Similarly, theories based on the drifts due to fluctuating fields also

claim better confinement for hydrogen than for deuterium. This lack of theoretical understanding provides us with further motivation.

Finally, our findings are summarized in Section 17 and some conclusions are drawn.

2 Ohmic discharges with carbonized or boronized wall conditioning

Ohmic ASDEX discharges with *carbonized* wall conditions have been analyzed for the parameter range 150 kA $\leq I_p \leq$ 440 kA, 1.9 T $\leq B_t \leq$ 2.45 T, and 0.8×10^{19} m$^{-3} \leq \overline{n}_e \leq 5.5 \times 10^{19}$ m^{-3}. The regression fits for various plasma parameters such as the Ohmic heating power P_{OH}, the total (E_0) and the electron (E_e) energy contents, the energy confinement time τ_E, the central (T_{e0}) and the volume-averaged ($\langle T_e \rangle$) electron temperatures, the temperature peaking $T_{e0}/\langle T_e \rangle$, the central ($n_{e0}$) and the volume-averaged ($\langle n_e \rangle$) electron densities, the density peaking $n_{e0}/\langle n_e \rangle$, the central ion temperature T_{i0}, and the sawtooth repetition time τ_{ST} as functions of I_p, B_t, $\overline{n}_e$, $Z_{\rm eff}$, and A_i are set out in Table 1. For simplicity, it is set $A_i = 1$ for hydrogen and $A_i = 2$ for deuterium discharges.[1]

For medium to high densities ($\overline{n}_e > 2.5 \times 10^{19}$ m^{-3}), i.e. in the Saturated Ohmic Confinement (SOC) regime, Table 1(b) gives the scalings that the isotope effect is most prominent in the sawtooth repetition rate

$$\tau_{ST} \propto I_p^0 \times B_t^0 \times \overline{n}_e^0 \times Z_{\rm eff}^{-0.61} \times A_i^{0.54},$$

in the energy confinement time

$$\tau_E \propto I_p^0 \times B_t^{0.18} \times \overline{n}_e^0 \times Z_{\rm eff}^{-0.27} \times A_i^{0.50},$$

and in the central electron temperature

$$T_{e0} \propto I_p^{0.31} \times B_t^{0.79} \times \overline{n}_e^{-0.63} \times A_i^{0.36};$$

the density dependent isotope behaviour is illustrated in Figure 1. Owing to the lower electron temperature in the case of hydrogen, the Ohmic heating power is larger in hydrogen than in deuterium plasmas, as illustrated in Figure 2(a). This figure shows data of Ohmic discharges in ASDEX with different density and $I_p = 425$ kA, $B_t = 2.2$ T. Impurity radiation is larger in deuterium than in hydrogen as a consequence of the better particle confinement; this is the case for all wall coatings. Whether a notable difference appears in $Z_{\rm eff}$ depends on the wall composition. A difference appears in case of the bare stainless steel wall; none in case of carbonized

[1] A more sophisticated analysis should work with the mean plasma mass per electron, i.e.

$$\left(\frac{A}{Z}\right)_{\rm eff} = \left(n_H + 2n_D + \frac{m_Z}{Z} n_Z\right) / \left(n_H + n_D + n_Z\right),$$

which is determined by the H/D ratio in the plasma, as measured by mass spectrometry, and an average impurity species with e.g. $m_Z = 2Z = 14$ as oxygen and carbon mixture.

(a)	const	I_p (kA)	B_t (T)	$\overline{n}_e$ (10^{19} m^{-3})	Z_{eff}	A_i	R
P_{OH} (MW)	9.93×10^{-4}	1.02	-0.45	0.26	0.24	-0.09	0.96
E_0 (kJ)	2.43×10^{-2}	1.12	-0.18	0.56	-0.14	0.21	0.97
E_e (kJ)	1.69×10^{-2}	1.12	0.00	0.38	-0.11	0.18	0.97
τ_E (ms)	$3.73 \times 10^{+1}$	0.00	0.27	0.39	-0.28	0.31	0.80
T_{e0} (eV)	$4.13 \times 10^{+1}$	0.49	0.73	-0.36	0.14	0.24	0.88
$\langle T_e \rangle$ (eV)	$6.14 \times 10^{+0}$	0.77	0.21	-0.37	0.12	0.17	0.92
$T_{e0}/\langle T_e \rangle$	$6.83 \times 10^{+0}$	-0.27	0.51	0.00	0.00	0.00	0.54
n_{e0} (10^{19} m^{-3})	$4.02 \times 10^{+0}$	-0.14	0.00	0.85	-0.25	0.02	0.97
$\langle n_e \rangle$ (10^{19} m^{-3})	2.31×10^{-1}	0.33	-0.17	0.68	-0.25	-0.12	0.93
$n_{e0}/\langle n_e \rangle$	$1.49 \times 10^{+1}$	-0.46	0.24	0.16	0.00	0.20	0.83
T_{i0} (eV)	$5.75 \times 10^{+1}$	0.40	0.36	0.10	0.00	0.00	0.81
τ_{ST} (ms)	$5.64 \times 10^{+1}$	-0.43	0.00	0.81	0.00	0.25	0.83

(b)	const	I_p (kA)	B_t (T)	$\overline{n}_e$ (10^{19} m^{-3})	Z_{eff}	A_i	R
P_{OH} (MW)	7.93×10^{-4}	1.09	-0.40	0.24	0.00	-0.22	0.96
E_0 (kJ)	5.74×10^{-2}	0.99	-0.13	0.43	-0.16	0.28	0.97
E_e (kJ)	1.40×10^{-2}	1.14	0.00	0.35	0.00	0.27	0.97
τ_E (ms)	$5.76 \times 10^{+1}$	0.00	0.18	0.00	-0.27	0.50	0.86
T_{e0} (eV)	$1.53 \times 10^{+2}$	0.31	0.79	-0.63	0.00	0.36	0.94
$\langle T_e \rangle$ (eV)	$5.92 \times 10^{+0}$	0.84	0.19	-0.62	0.00	0.19	0.88
$T_{e0}/\langle T_e \rangle$	$5.62 \times 10^{+1}$	-0.67	0.66	0.00	0.00	0.11	0.87
n_{e0} (10^{19} m^{-3})	$4.66 \times 10^{+0}$	-0.21	0.14	0.84	-0.11	0.10	0.93
$\langle n_e \rangle$ (10^{19} m^{-3})	9.68×10^{-2}	0.42	-0.26	1.01	-0.10	-0.12	0.97
$n_{e0}/\langle n_e \rangle$	$3.73 \times 10^{+1}$	-0.59	0.37	-0.17	0.00	0.25	0.94
T_{i0} (eV)	$1.13 \times 10^{+2}$	0.29	0.55	-0.28	0.00	0.16	0.72
τ_{ST} (ms)	$1.57 \times 10^{+1}$	0.00	0.00	0.00	-0.61	0.54	0.82

Table 1: Exponents of the regression analysis in the form const $\times I_p^{\alpha \pm \delta\alpha} \times B_t^{\beta \pm \delta\beta} \times \ldots$ for carbonized Ohmic ASDEX discharges. R denotes the regression coefficient. Results for (a) $\overline{n}_e \leq 2.5 \times 10^{19}$ m^{-3} (LOC) and (b) $\overline{n}_e > 2.5 \times 10^{19}$ m^{-3} (SOC).

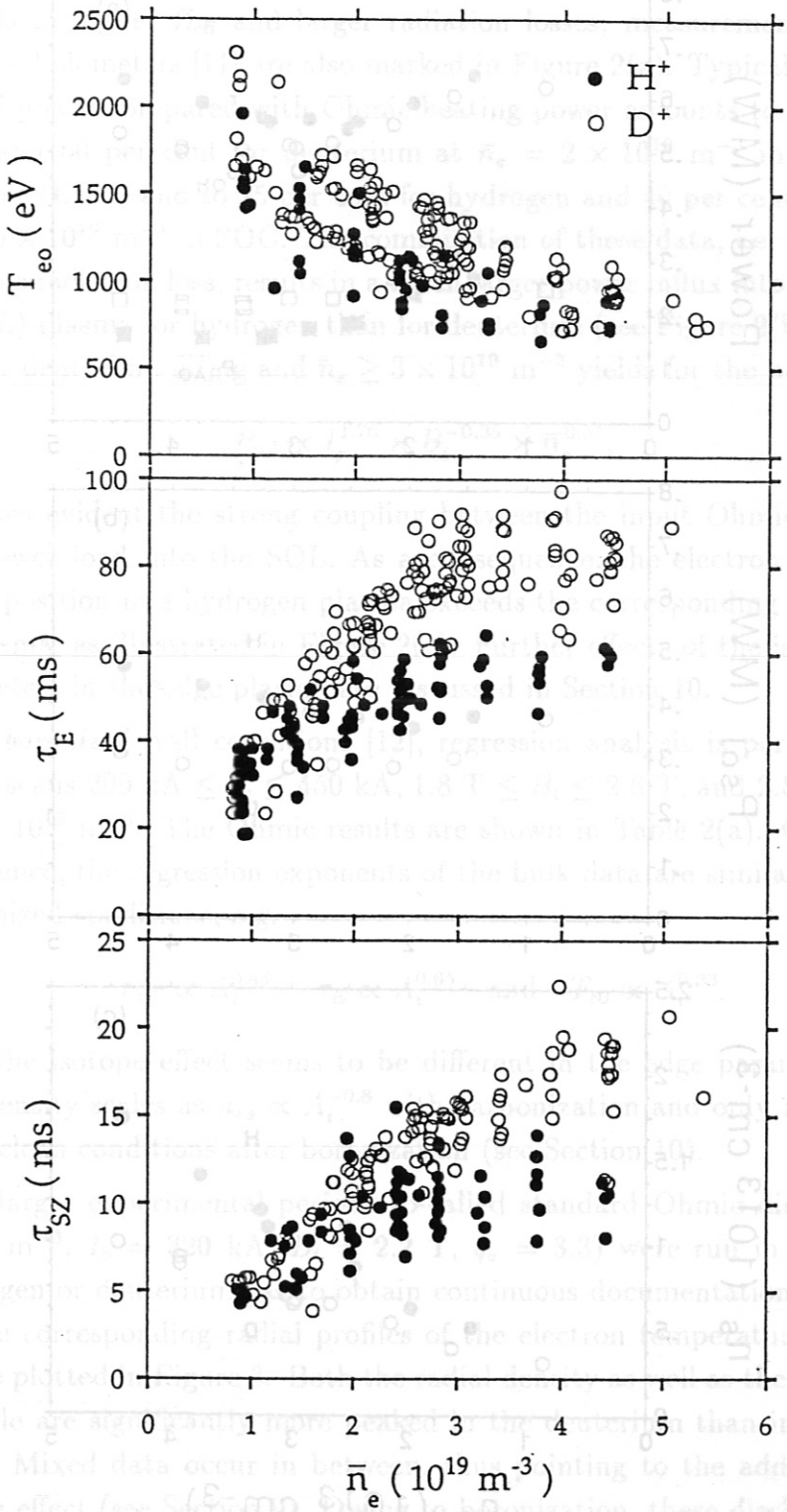

Figure 1: Density scans of (a) central electron temperature T_{e0}, (b) energy confinement time τ_E, and (c) sawtooth repetition time τ_{SZ} for both hydrogen and deuterium filling ($2.5 \leq q_a \leq 4.0$).

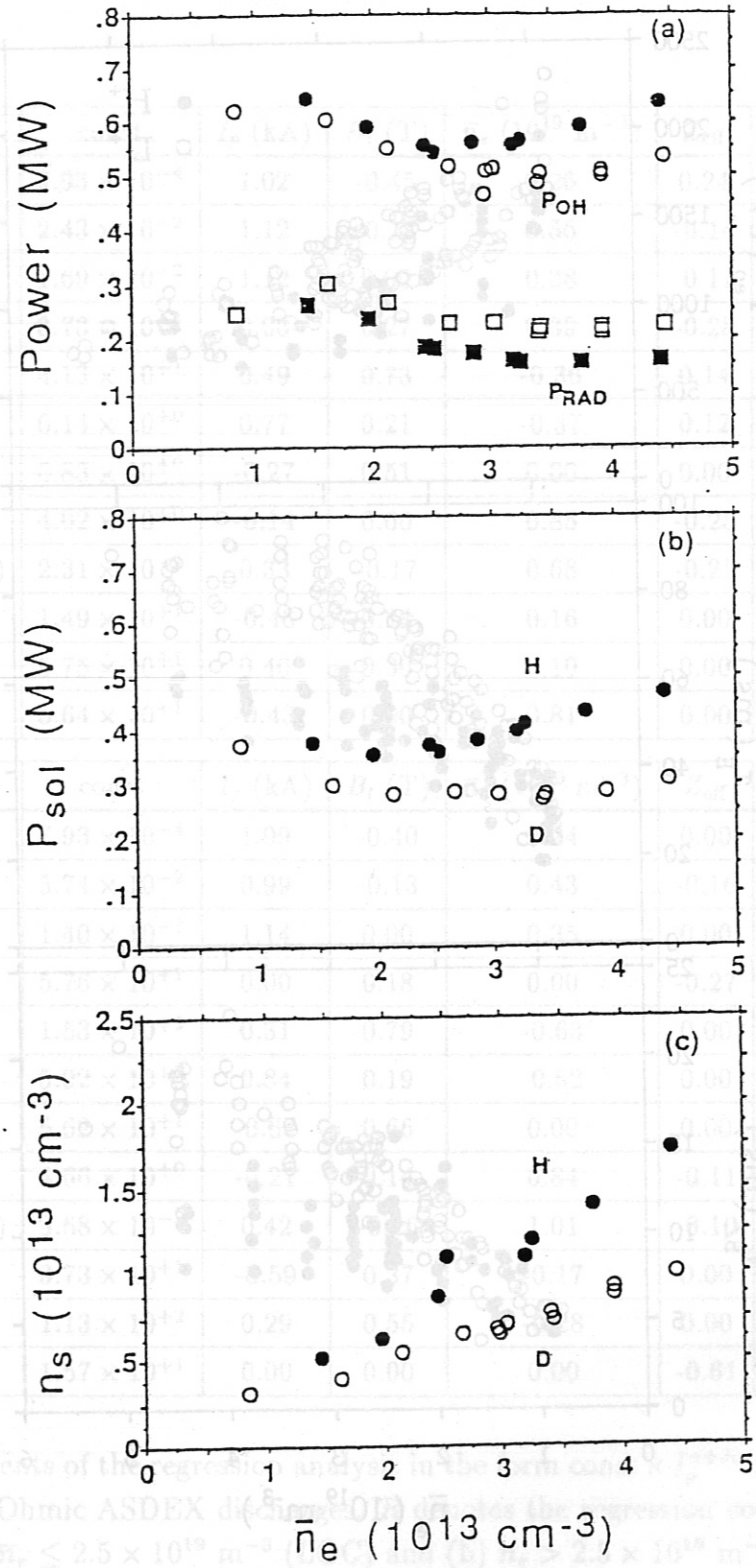

Figure 2: Density scan under carbonized ASDEX conditions ($I_p = 425$ kA, $B_t = 2.2$ T) for both hydrogen and deuterium filling.
(a) Ohmic heating power and total radiation loss, (b) power influx into the SOL, (c) electron density at the separatrix position.

wall. In addition, the impurity content for deuterium is larger than for hydrogen, which leads to higher $Z_{\rm eff}$ and larger radiation losses; measurements of the total radiation by bolometers [11] are also marked in Figure 2(a). Typically, the fraction of radiated power compared with Ohmic heating power amounts to 40 per cent for hydrogen and 50 per cent for deuterium at $\overline{n}_e = 2 \times 10^{19}$ m^{-3} in Linear Ohmic Confinement (LOC) and to 25 per cent for hydrogen and 40 per cent for deuterium at $\overline{n}_e = 4.5 \times 10^{19}$ m^{-3} in SOC. The combination of these data, i.e. Ohmic heating power minus radiation loss, results in a much larger power influx into the Scrape-Off Layer (SOL) plasma for hydrogen than for deuterium (see Figure 2(b)). Regression analysis for deuterium filling and $\overline{n}_e \geq 3 \times 10^{19}$ m^{-3} yields for the power flux

$$P_{\rm sol} \propto I_p^{1.76} \times B_t^{-0.35} \times \overline{n}_e^{0.37},$$

which makes evident the strong coupling between the input Ohmic data (I_p, B_t) and the power load into the SOL. As a consequence, the electron density at the separatrix position in a hydrogen plasma exceeds the corresponding value of a deuterium plasma, as illustrated in Figure 2(c). Further effects of the isotope mass on the parameters in the edge plasma are discussed in Section 10.

With *boronized* wall conditions [12], regression analysis is performed for the parameter scans 200 kA $\leq I_p \leq$ 450 kA, 1.8 T $\leq B_t \leq$ 2.8 T, and 2.5×10^{19} m$^{-3} \leq \overline{n}_e \leq 5.5 \times 10^{19}$ m^{-3}. The Ohmic results are shown in Table 2(a). Concerning the A_i dependence, the regression exponents of the bulk data are similar for boronized and carbonized conditions, e.g.

$$\tau_{ST} \propto A_i^{0.44}, \quad \tau_E \propto A_i^{0.65} \quad \text{and} \quad T_{e0} \propto A_i^{0.33}.$$

However, the isotope effect seems to be different in the edge parameters, namely the edge density scales as $n_{es} \propto A_i^{-0.8}$ with carbonization and only as $n_{es} \propto A_i^{-0.29}$ under the clean conditions after boronization (see Section 10).

Over larger experimental periods so-called standard Ohmic discharges ($\overline{n}_e = 3.0 \times 10^{19}$ m^{-3}, $I_p = 320$ kA, $B_t = 2.2$ T, $q_a = 3.3$) were run in ASDEX in either hydrogen or deuterium gas to obtain continuous documentation of the isotope effect. The corresponding radial profiles of the electron temperature and electron density are plotted in Figure 3. Both the radial density as well as the radial temperature profile are significantly more peaked in the deuterium than in the hydrogen discharge. Mixed data occur in between, thus pointing to the additive nature of the isotope effect (see Section 9). Owing to boronization, these discharges are very clean and have $Z_{\rm eff}$ values close to 1. Figure 4 shows the radial profile of $Z_{\rm eff}$ as obtained from bremsstrahlung measurements ([13];[14]) for the same discharges as in Figure 3. Whereas the central value $Z_{\rm eff}(0)$ amounts to 1.8 for deuterium and

(a)	const	I_p (kA)	B_t (T)	$\overline{n}_e$ (10^{19} m^{-3})	A_i	R
P_{OH} (MW)	5.62×10^{-4}	1.13	-0.35	0.26	-0.18	0.99
E_0 (kJ)	1.55×10^{-2}	1.19	-0.32	0.44	0.47	0.98
E_e (kJ)	$1.32 \times 10^{+2}$	1.17	0.00	0.44	0.36	1.00
τ_E (ms)	$3.80 \times 10^{+1}$	0.00	0.00	0.21	0.65	0.92
T_{e0} (eV)	$1.35 \times 10^{+2}$	0.29	0.72	-0.50	0.33	0.97
$\langle T_e \rangle$ (eV)	$2.34 \times 10^{+0}$	0.96	0.00	-0.55	0.29	0.98
$T_{e0}/\langle T_e \rangle$	$5.75 \times 10^{+1}$	-0.66	0.68	0.00	0.05	0.95
n_{e0} (10^{19} m^{-3})	$2.57 \times 10^{+0}$	-0.13	0.18	0.91	0.08	0.99
$\langle n_e \rangle$ (10^{19} m^{-3})	1.91×10^{-1}	0.27	0.00	0.98	-0.12	0.97
$n_{e0}/\langle n_e \rangle$	$1.12 \times 10^{+1}$	-0.40	0.28	0.08	0.17	0.90
T_{i0} (eV)	$3.55 \times 10^{+2}$	0.17	0.35	-0.42	0.00	
τ_{ST} (ms)	$1.20 \times 10^{+2}$	-0.48	0.00	0.27	0.44	

(b)	const	I_p (kA)	B_t (T)	$\overline{n}_e$ (10^{19} m^{-3})	A_i	R
E_0 (kJ)	2.40×10^{-1}	0.87	-0.14	0.14	0.44	0.98
E_e (kJ)	5.25×10^{-2}	0.88	0.09	0.52	0.24	0.99
τ_E (ms)	$1.10 \times 10^{+0}$	0.55	-0.14	0.09	0.34	0.97
T_{e0} (eV)	$2.63 \times 10^{+2}$	0.27	0.55	-0.46	0.25	0.89
$\langle T_e \rangle$ (eV)	$6.61 \times 10^{+0}$	0.83	0.11	-0.49	0.13	0.97
$T_{e0}/\langle T_e \rangle$	$3.98 \times 10^{+1}$	-0.56	0.44	0.00	0.12	0.91
n_{e0} (10^{19} m^{-3})	$1.45 \times 10^{+0}$	0.00	0.09	0.90	0.07	0.99
$\langle n_e \rangle$ (10^{19} m^{-3})	5.13×10^{-1}	0.08	-0.06	1.11	-0.15	0.99
$n_{e0}/\langle n_e \rangle$	$2.82 \times 10^{+0}$	-0.11	0.14	-0.21	0.22	0.88
τ_{ST} (ms)	$1.10 \times 10^{+1}$	0.15	0.23	-0.39	0.46	

Table 2: Exponents of the regression analysis in the form const $\times I_p^{\alpha} \times B_t^{\beta} \times \ldots$ for boronized ASDEX discharges. R denotes the regression coefficient. Results for (a) Ohmic saturated phase and (b) NI phase ($P_{NI} = 1.6$ MW).

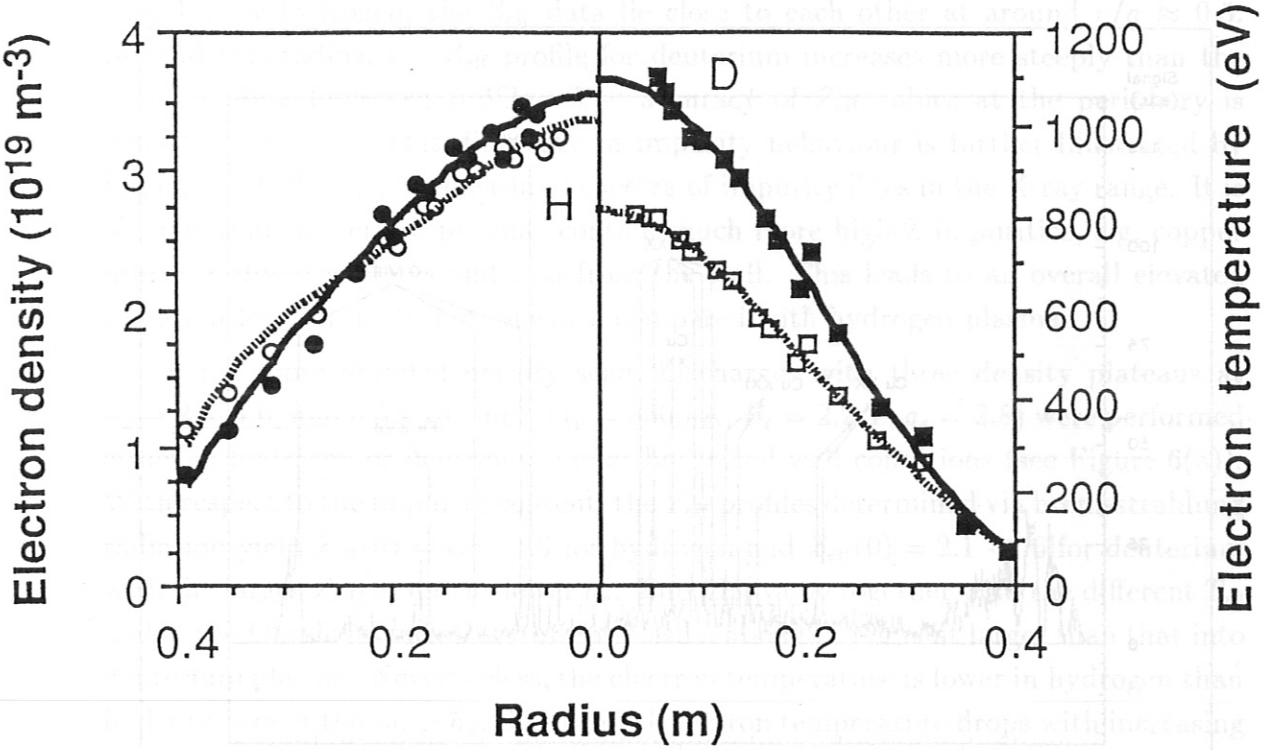

Figure 3: Radial profiles of the electron density and temperature for Ohmic standard discharges in ASDEX ($\overline{n}_e = 3.0 \times 10^{19}$ m^{-3}, $I_p = 320$ kA, $B_t = 2.2$ T, $q_a = 3.3$) under boronized wall conditions.

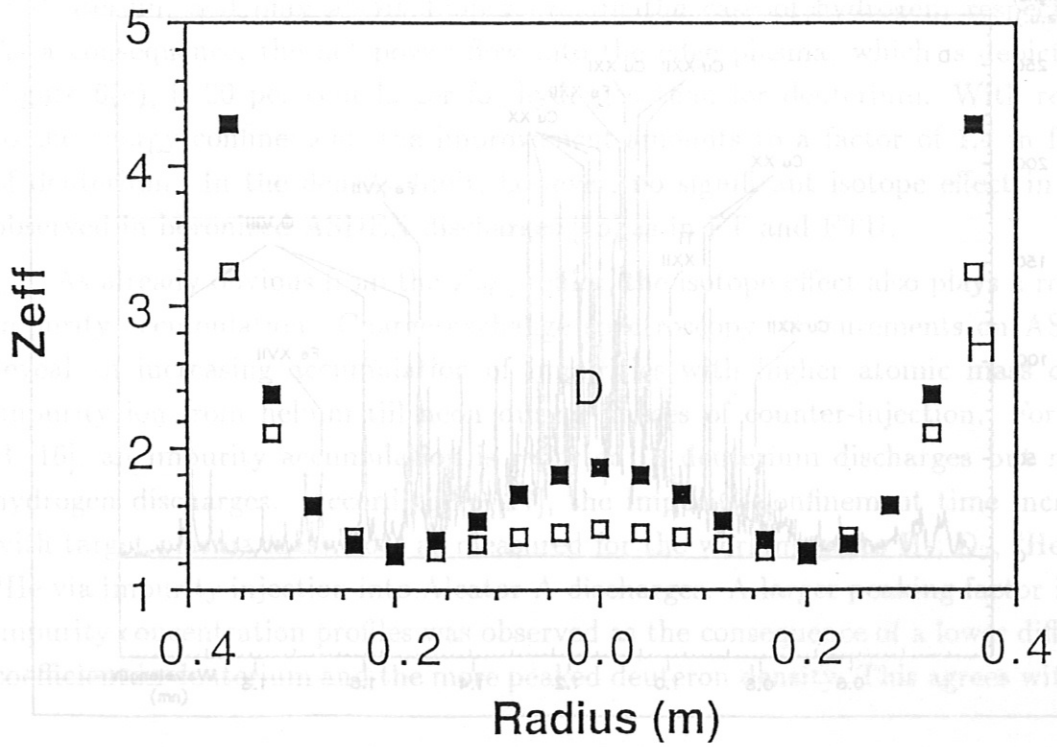

Figure 4: Radial profile of Z_{eff} for the same Ohmic standard discharges as in Figure 3. The profiles are symmetrized by Abel inversion.

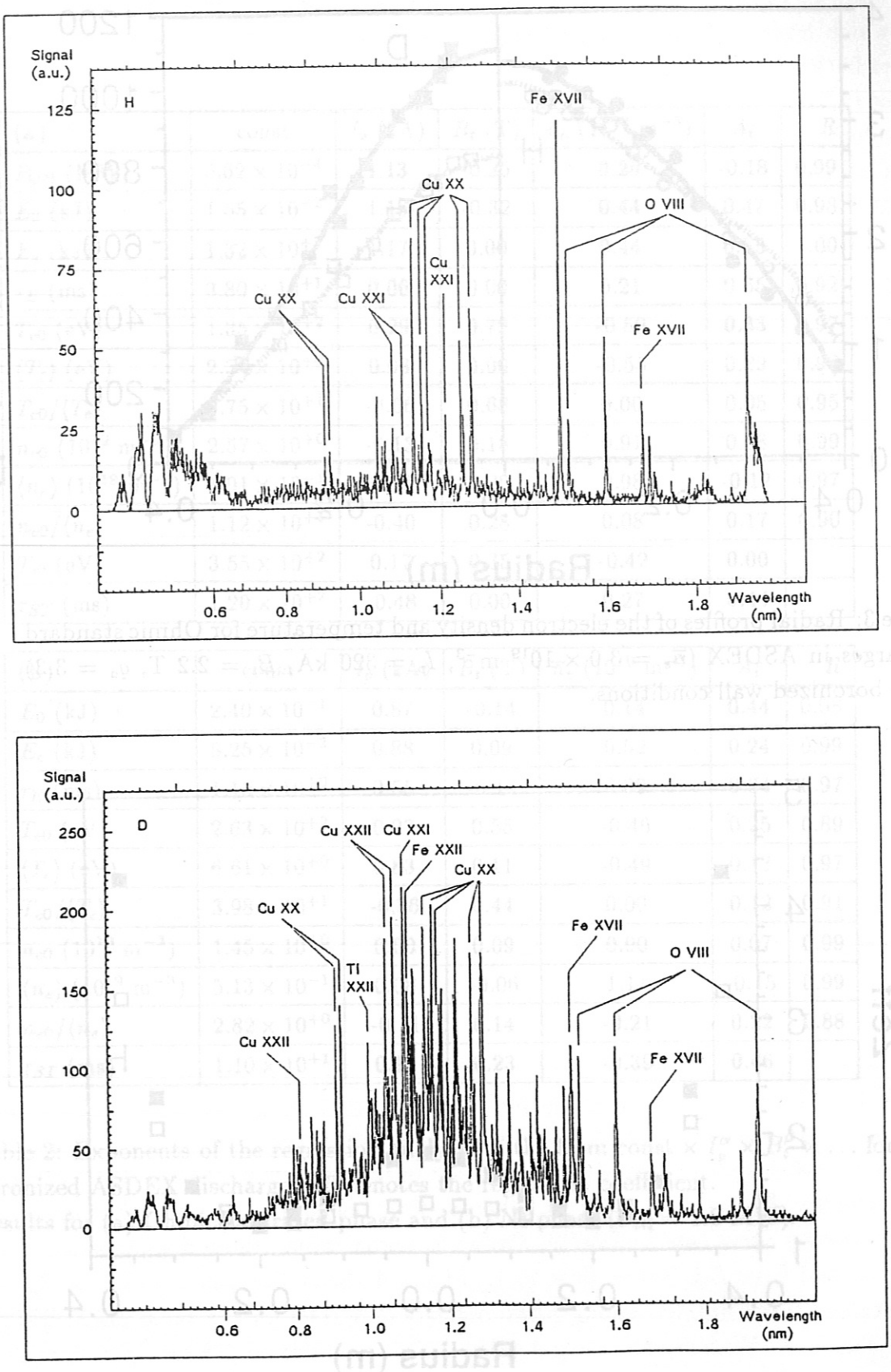

Figure 5: X-ray spectra of high-Z impurities for the same Ohmic standard discharges as in Figure 3. (a) Hydrogen and (b) deuterium spectrum.

only 1.4 for hydrogen, the Z_{eff} data lie close to each other at around $r/a \approx 0.5$. Beyond this radius, the Z_{eff} profile for deuterium increases more steeply than the corresponding hydrogen profile. The accuracy of Z_{eff} values at the periphery is doubtful, however. This difference in impurity behaviour is further illustrated by Figure 5, which presents measured spectra of impurity lines in the X-ray range. It is obvious that deuterium plasmas contain much more high-Z impurities, e.g. copper from the divertor plates and iron from the wall. This leads to an overall elevated radiation level in deuterium plasmas compared with hydrogen plasmas.

For a more detailed density scan, discharges with three density plateaus at $\overline{n}_e = 2.5$, 4.0, and 5.5×10^{19} m^{-3} ($I_p = 380$ kA, $B_t = 2.2$ T, $q_a = 2.8$) were performed either in hydrogen or deuterium under boronized wall conditions (see Figure 6(a)). With respect to the impurity content, the Z_{eff} profiles determined via bremsstrahlung radiation yield $Z_{\text{eff}}(0) = 1.6$ - 1.3 for hydrogen and $Z_{\text{eff}}(0) = 2.1$ - 1.6 for deuterium with the larger $Z_{\text{eff}}(0)$ for the lower $\overline{n}_e$. This Z_{eff} value together with the different T_{e0} makes the Ohmic input into hydrogen plasma about 15 per cent larger than that into deuterium plasma. Nevertheless, the electron temperature is lower in hydrogen than in deuterium at the same $\overline{n}_e$. The central electron temperature drops with increasing density from 850 to 650 eV for hydrogen and from 1040 to 750 eV for deuterium as illustrated in Figure 6(b). The profiles of the total radiation are consistent with these measurements since indeed higher radiation losses for deuterium than for hydrogen show up with maximum values around the separatrix position. The radiation loss in the bulk plasma reaches about 25 per cent of the Ohmic heating in the case of deuterium and only about 15 per cent in the case of hydrogen, respectively. As a consequence, the net power flow into the edge plasma, which is depicted in Figure 6(c), is 20 per cent larger for hydrogen than for deuterium. With respect to the energy confinement, the improvement amounts to a factor of 1.4 in favour of deuterium. In the density limit, however, no significant isotope effect in τ_E is observed in boronized ASDEX discharges [15] as in FT and FTU.

As already obvious from the Z_{eff} profiles, the isotope effect also plays a role for impurity accumulation. Charge exchange spectroscopy measurements on ASDEX reveal an increasing accumulation of impurities with higher atomic mass of the impurity ion from helium till neon during phases of counter-injection. For ISX-B [16], an impurity accumulation is reported in deuterium discharges but not in hydrogen discharges. According to [17], the impurity confinement time increases with target plasma mass, too, as measured for the working gases H_2, D_2, ^{3}He, and ^{4}He via impurity injection into Alcator-A discharges. A larger peaking factor in the impurity concentration profiles was observed as the consequence of a lower diffusion coefficient in deuterium and the more peaked deuteron density. This agrees with the

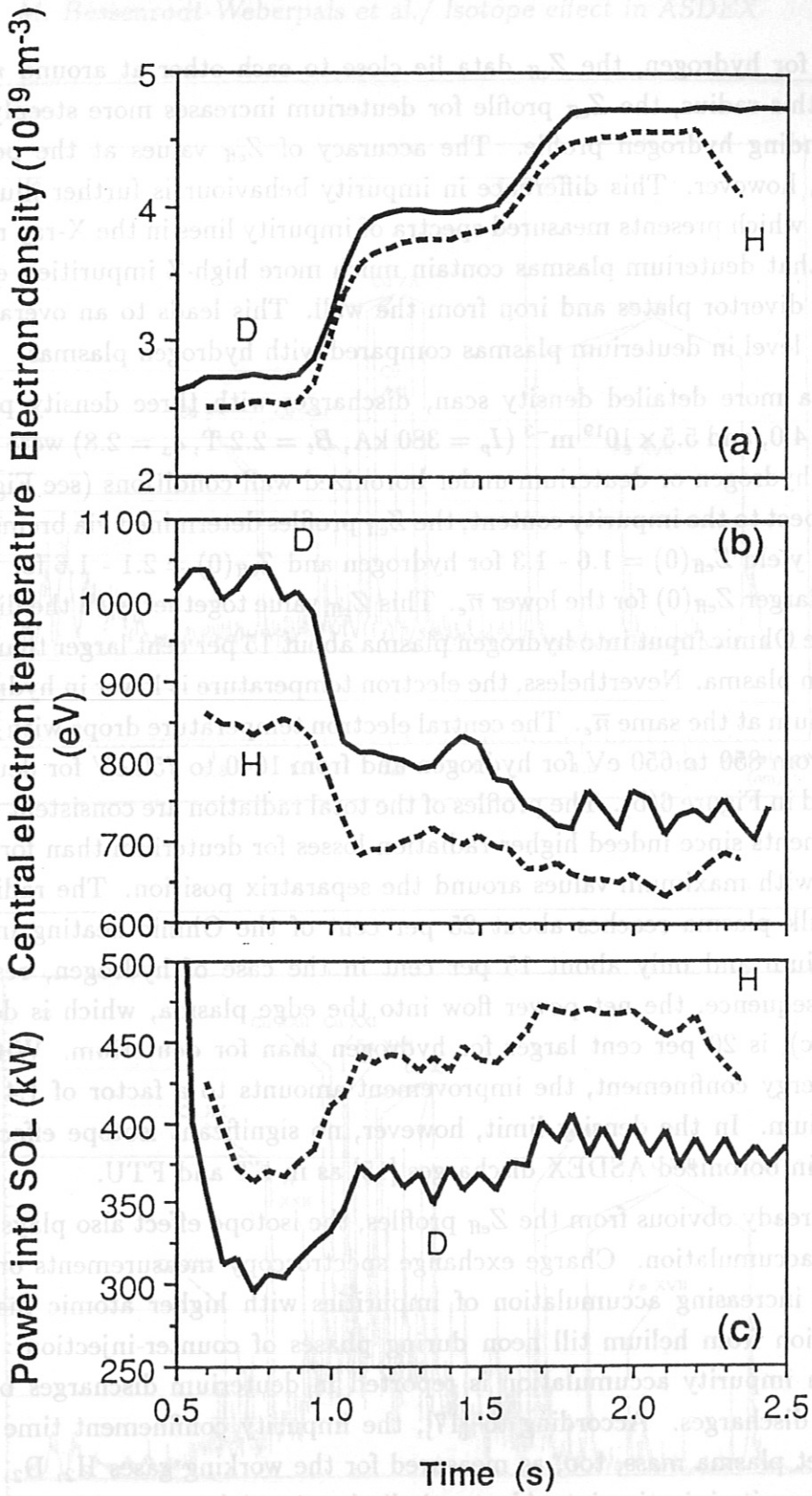

Figure 6: Temporal evolution of ASDEX discharges (I_p = 380 kA, B_t = 2.2 T, q_a = 2.8) with three density plateaus at $\overline{n}_e$ = 2.5, 4.0 and 5.5 × 10^{19} m^{-3} for either hydrogen (#28554) or deuterium (#30451) filling under boronized wall conditions. (In all cases, the origin is suppressed.) (a) Electron density integrated over the line of sight, (b) central electron temperature, (c) power influx into the SOL $P_{sol} = P_{tot} - P_{rad,main}$.

mixed neoclassical estimate of the hydrogen isotope peaking via $v^{(neo)}/D^{(an)}$ which gives

$$\frac{v^{(neo)}/D^{(an)}(D)}{v^{(neo)}/D^{(an)}(H)} > 1,$$

since $v^{(neo)}(D)/v^{(neo)}(H) > 1$ and $D^{(an)}(D)/D^{(an)}(H) < 1$, and the assumption of strong collisional coupling between hydrogen and impurity species.

3 Discharges with additional heating in L-mode

In order to extend the isotope investigations to larger heating power, we perform discharges with additional heating via the injection of energetic neutrals or via waves at either the ion cyclotron resonance or the lower hybrid resonance. The preceding chapter showed that the isotope effect is a well established scaling parameter of Ohmic plasmas and there is evidence that it becomes weaker under auxiliary heating conditions. Since Ohmic plasmas are subjected to power degradation which is compensated by the current (if Ohmic heating power is varied by current) [18], a mechanism, which changes confinement, changes consequently the mean electron temperature will have a more pronounced effect under Ohmic conditions. As the Ohmic heating power is reduced in case of a confinement improvement the overall effect on τ_E is larger under Ohmic conditions because less power degradation occurs: $\tau_E \propto A_i^{\alpha}$ transfers into $\tau_E \propto A_i^{\frac{10}{7}\alpha}$ under Ohmic conditions, where P_{OH} is not used as an explicit regression variable besides I_p. Under L-mode conditions, a scaling $\tau_E \propto A_i^{0.3}$ transfers into a scaling $\tau_E \propto A_i^{0.5}$ under Ohmic conditions. There is agreement with experimental observation. An alternative possibility is that the isotope effect on confinement disappears when the turbulence of the plasma increases e.g. owing to stronger auxiliary heating under L-mode conditions. Indicative of this possibility is the seemingly larger isotope effect under H-mode conditions.

The energy confinement time of L-mode discharges with neutral injection (NI) sensitively depends on the ion masses of the background plasma and beam component. In these discharges, isotopic differences in radiation levels also exist, but are negligible for the τ_E evaluation. For sufficiently high heating powers, ASDEX studies (e.g. [19]) reveal an L-mode ordering of the form

$$\tau_E(\mathrm{H}^0 \rightarrow \mathrm{H}^+)[\mathrm{L-mode}]$$
$$< \tau_E(\mathrm{D}^0 \rightarrow \mathrm{H}^+)[\mathrm{L-mode}] \approx \tau_E(\mathrm{H}^0 \rightarrow \mathrm{D}^+)[\mathrm{L-mode}]$$
$$< \tau_E(\mathrm{D}^0 \rightarrow \mathrm{D}^+)[\mathrm{L-mode}],$$

i.e. pure hydrogen conditions give the worst confinement and pure deuterium conditions the best, where mixed data lie in between (see Figure 7 and Table 2(b)); Section 9 comprehends the observations of the additive nature of the isotope effects. The different slowing down of beam particles can be also taken into consideration by comparing pairs with equal beam injection which is expressed by the two relations

$$\tau_E(\mathrm{H}^0 \rightarrow \mathrm{H}^+)[\mathrm{L-mode}] < \tau_E(\mathrm{H}^0 \rightarrow \mathrm{D}^+)[\mathrm{L-mode}]$$

and

$$\tau_E(\mathrm{D}^0 \rightarrow \mathrm{H}^+)[\mathrm{L-mode}] < \tau_E(\mathrm{D}^0 \rightarrow \mathrm{D}^+)[\mathrm{L-mode}].$$

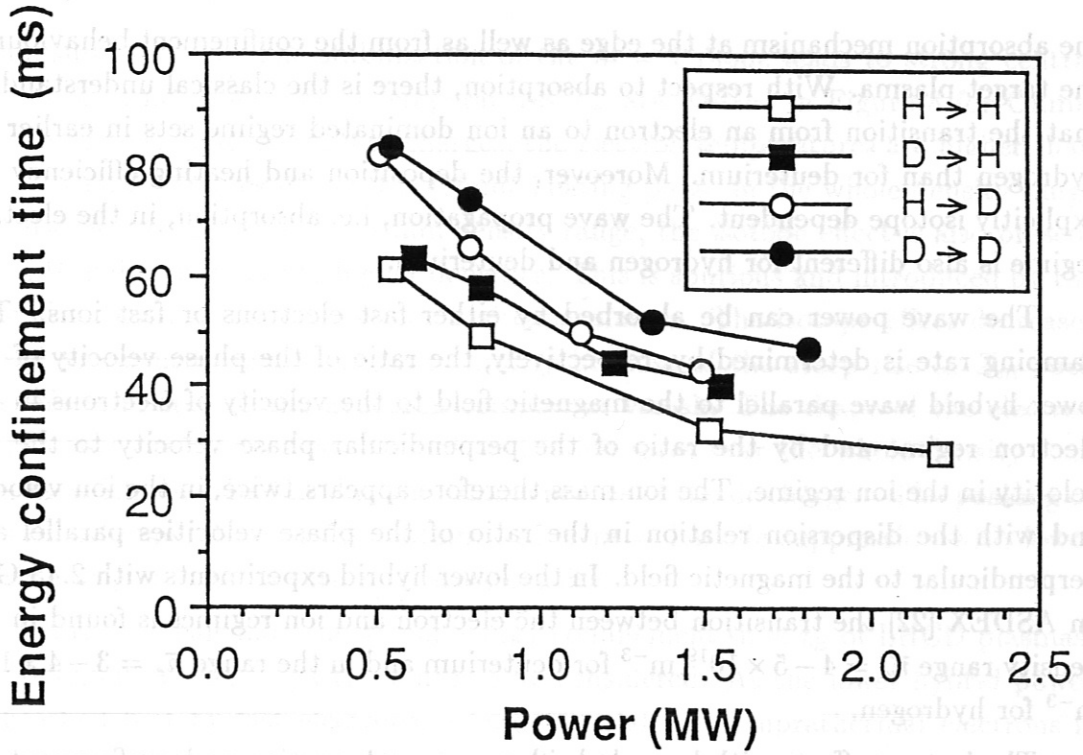

Figure 7: Energy confinement time as a function of heating power with either hydrogen or deuterium injection into either hydrogen or deuterium plasmas.

With respect to edge parameters, the isotope effect on the separatrix density fades away. A possible explanation of the model given in Section 10 is the high power influx into the SOL during neutral injection, which greatly exceeds the Ohmic values.

Isotope effects are also observed with ion cyclotron resonance heating, ICRH, in ASDEX. However, the study is restricted by the necessity of using different scenarios for deuterium and hydrogen: hydrogen minority heating is only possible in deuterium plasma, eventually combined with deuterium neutral injection, whereas hydrogen second harmonic heating works satisfactorily in pure hydrogen and in hydrogen/deuterium mixtures, up to deuterium concentration of 70 %. Therefore, the study of isotope effects with ICRH can only be performed for second harmonic heating in the gas mixture indicated above, implying errors on the effective mass estimate and consequently on the mass scaling. Moreover, the power absorption might vary somewhat with the mixture, introducing an additional error. Despite these uncertainties, an isotope effect on confinement comparable to that observed in the Ohmic plasmas and beam-heated plasmas seems to exist in ICRH heated discharges [20]; [21], supporting the generality of this effect in ASDEX.

With regard to lower hybrid waves, isotope effects seem to originate both from

the absorption mechanism at the edge as well as from the confinement behaviour of the target plasma. With respect to absorption, there is the classical understanding that the transition from an electron to an ion dominated regime sets in earlier for hydrogen than for deuterium. Moreover, the deposition and heating efficiency are explicitly isotope dependent. The wave propagation, i.e. absorption, in the electron regime is also different for hydrogen and deuterium.

The wave power can be absorbed by either fast electrons or fast ions. The damping rate is determined by, respectively, the ratio of the phase velocity of the lower hybrid wave parallel to the magnetic field to the velocity of electrons in the electron regime and by the ratio of the perpendicular phase velocity to the ion velocity in the ion regime. The ion mass therefore appears twice, in the ion velocity and with the dispersion relation in the ratio of the phase velocities parallel and perpendicular to the magnetic field. In the lower hybrid experiments with 2.45 GHz on ASDEX [22] the transition between the electron and ion regimes is found in the density range $\overline{n}_e = 4 - 5 \times 10^{19}$ m^{-3} for deuterium and in the range $\overline{n}_e = 3 - 4 \times 10^{19}$ m^{-3} for hydrogen.

The isotope effects with lower hybrid waves on absorption and confinement are discussed for a density scan with lower hybrid current drive (LHCD) in the density range $\overline{n}_e = 1.2 - 4 \times 10^{19}$ m^{-3}. Lower hybrid waves were injected with a phasing of $\Delta\Phi = 90°(N_{\|} = 2.2)$ and two steps in power, each of 500 ms duration. Steady-state conditions are attained in all cases. The measurements show an Ohmic power drop during LHCD which decreases with increasing density according to the density dependence of the LH-driven current:

$$I_{\mathrm{LH}} = \eta P_{\mathrm{LH}}/(n_e R)$$

for both hydrogen isotopes. The LH-driven current shows the same density dependence for deuterium and hydrogen discharges up to a density $\overline{n}_e = 4 \times 10^{19}$ m^{-3}. At the highest density of $\overline{n}_e = 4 \times 10^{19}$ m^{-3}, however, the hydrogen measurements drop clearly below those for deuterium. At this value, strongly enhanced fluxes of energetic neutrals are observed on the neutral particle analyzer. The density limit for the electron regime has therefore been exceeded in this case and the lower hybrid waves start to be absorbed by edge ions rather than by electrons.

The degraded current drive efficiency in hydrogen at this density results also in reduced profile control capability. Sawteeth and $m = 1$ modes are stabilized in deuterium up to $\overline{n}_e = 4 \times 10^{19}$ m^{-3}, while in hydrogen this is achieved only up to $\overline{n}_e = 3 \times 10^{19}$ m^{-3}. The stabilization originates from a broadening of the current density profile in the central plasma region. With the reduced current drive efficiency in hydrogen at high density the LH-driven current is too small to modify the current

profile substantially. The stabilization of the $m = 1$ mode leads to strong central electron heating. The central temperatures T_{e0} are plotted in Figure 8 for Ohmic and LH phases. In deuterium discharges, the electron temperatures are higher than in hydrogen discharges during the Ohmic heating phase in the whole density range (see also Section 2). In the medium density range, the isotope effect is also present with LH and it increases to higher densities. This is spurious and introduced by the wave absorption at the edge of the hydrogen plasma. The isotope effect decreases toward low density and high power mostly because of the steep rise in Z_{eff} such that effects related to the hydrogen component vanish. The shape of the electron temperature profile does not depend on the ion mass over the whole density scan from $\overline{n}_e = 1.2 - 4 \times 10^{19}$ m^{-3} in the Ohmic phases of the discharges. The peaking of the radial temperature profile, obtained after $m = 1$ mode suppression with lower hybrid waves, decreases with increasing density.

In order to calculate the global energy confinement time τ_E of LHCD plasmas, the contribution of fast particles has to be considered. As the lower hybrid power is absorbed first by fast electrons, a large population of suprathermal electrons is generated and the energy distribution of the electrons becomes anisotropic with a major contribution in the direction parallel to the magnetic field. From magnetic measurements of equilibrium and diamagnetic beta values the different components and then the total energy content of all species in the plasma are determined. With the total energy content containing bulk and tail electrons the global energy confinement time τ_E is eventually calculated. Figure 9 shows the density dependence of τ_E for Ohmic and LHCD plasmas. The linear dependence $\tau_E \propto \overline{n}_e$ found in Ohmic phases in the density range $\overline{n}_e \leq 3 \times 10^{19}$ m^{-3} is reduced with increasing LH power. For Ohmic conditions, τ_E is higher in deuterium than in hydrogen for the whole density range. Here, the higher energy confinement times of deuterium result in both lower Ohmic input power and higher energy content. With lower hybrid waves as with NI, the superiority of deuterium reduces with increasing power level. With LHCD the Ohmic input power is decreased and replaced by LH power. The LHCD efficiency does not depend on the ion mass in the electron region, and therefore the LH input power is independent of the ion mass, too. On the other hand, also the enhanced electron heating after mode stabilization is similar in hydrogen and deuterium discharges. A weaker isotope effect is therefore found in plasmas dominated by LHCD and electron heating by the absorbed lower hybrid waves. At high density a degradation of energy confinement is observed in hydrogen compared with deuterium discharges with high power LHCD. There, however, the wave absorption regime has changed and damping is dominated by the generation of fast ions.

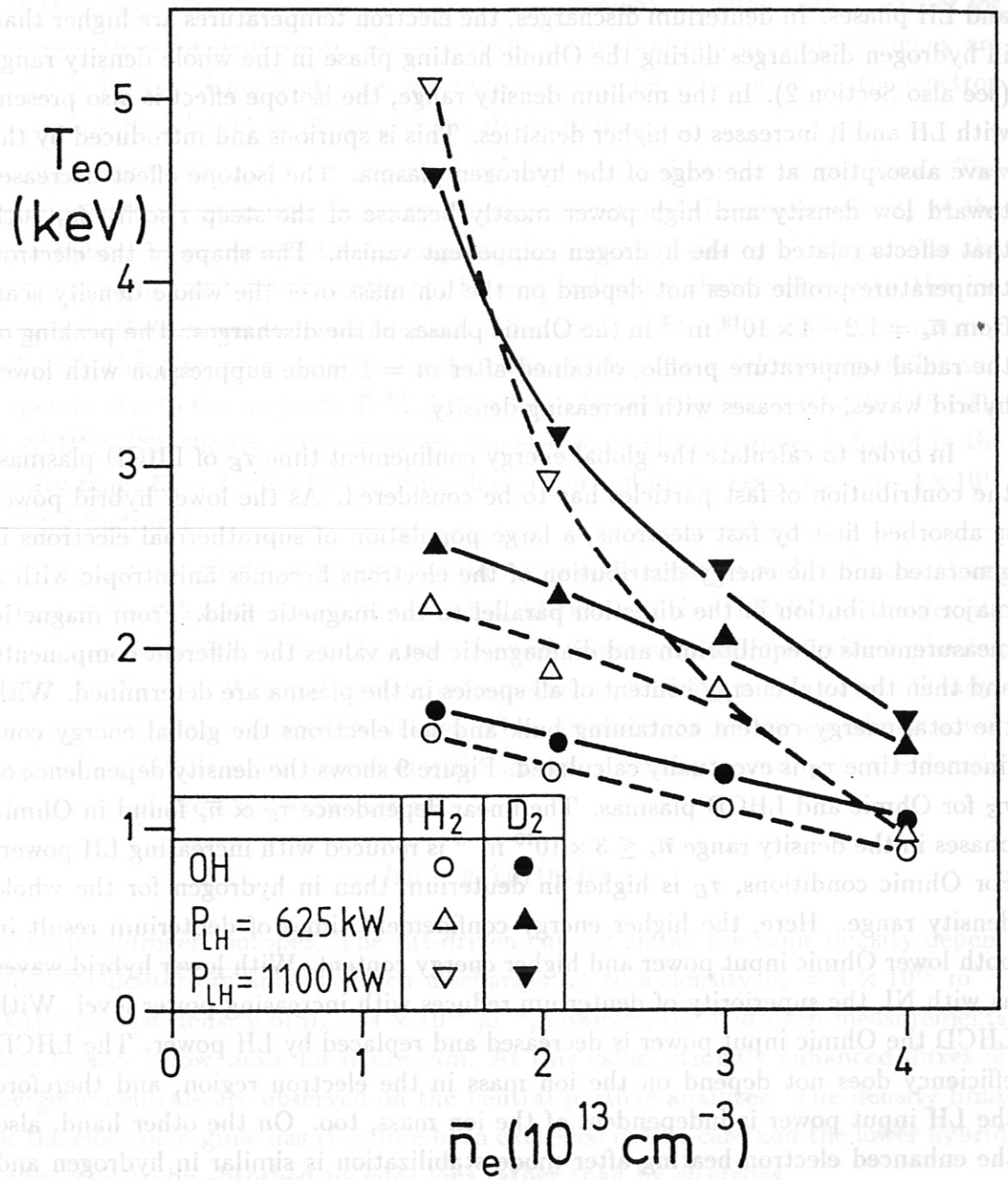

Figure 8: Central electron temperature as a function of electron density $\overline{n}_e$ for Ohmic and lower hybrid heating.

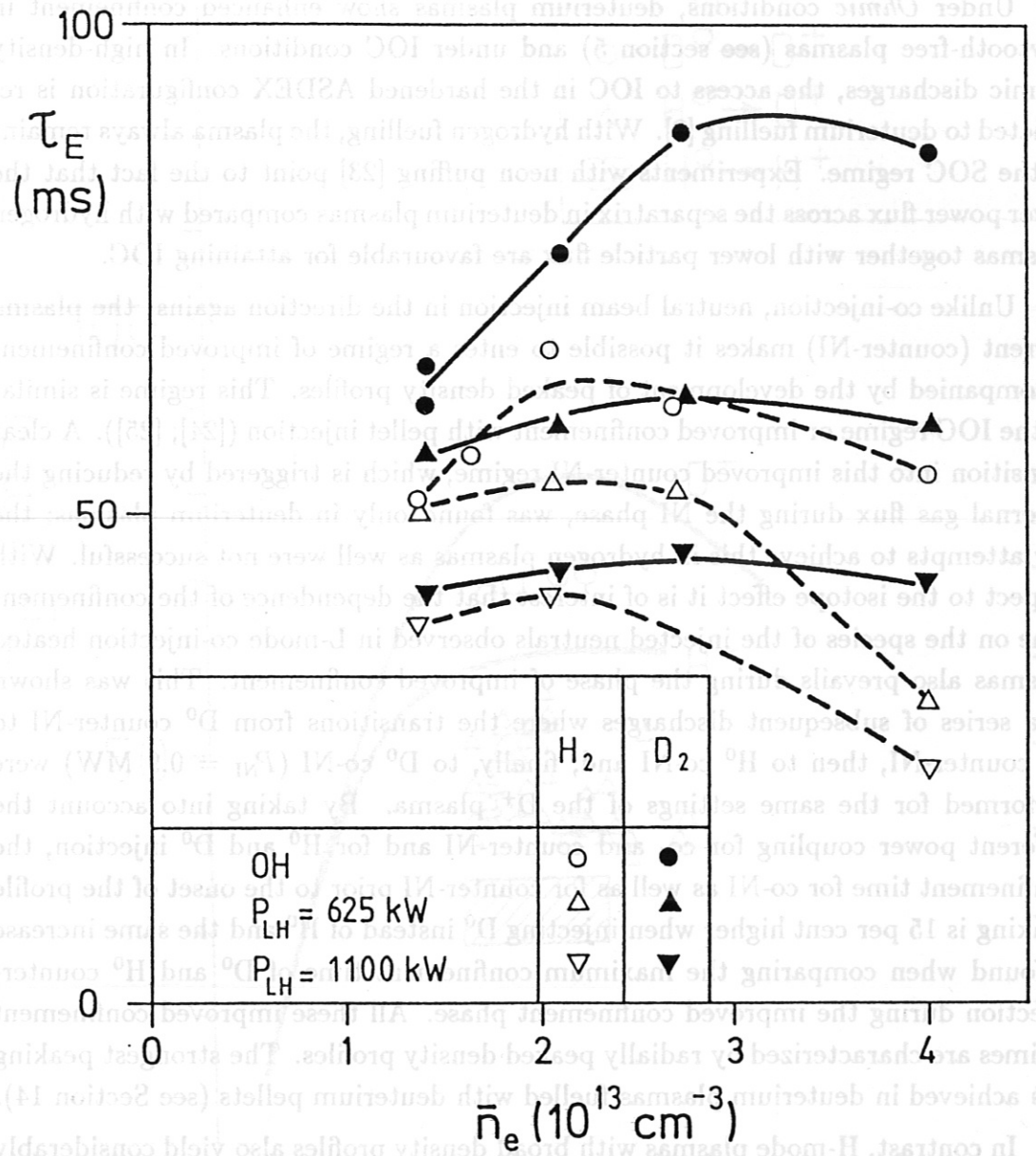

Figure 9: Energy confinement time as a function of electron density $\overline{n}_e$ for Ohmic and lower hybrid heating.

4 Improved confinement regimes

The isotope mix is a decisive parameter for many improved confinement scenarios.

Under *Ohmic* conditions, deuterium plasmas show enhanced confinement in sawtooth-free plasmas (see section 5) and under IOC conditions. In high-density Ohmic discharges, the access to IOC in the hardened ASDEX configuration is restricted to deuterium fuelling [2]. With hydrogen fuelling, the plasma always remains in the SOC regime. Experiments with neon puffing [23] point to the fact that the lower power flux across the separatrix in deuterium plasmas compared with hydrogen plasmas together with lower particle flux are favourable for attaining IOC.

Unlike co-injection, neutral beam injection in the direction against the plasma current (counter-NI) makes it possible to enter a regime of improved confinement accompanied by the development of peaked density profiles. This regime is similar to the IOC regime or improved confinement with pellet injection ([24]; [25]). A clear transition into this improved counter-NI regime, which is triggered by reducing the external gas flux during the NI phase, was found only in deuterium plasmas; the few attempts to achieve this in hydrogen plasmas as well were not successful. With respect to the isotope effect it is of interest that the dependence of the confinement time on the species of the injected neutrals observed in L-mode co-injection heated plasmas also prevails during the phase of improved confinement. This was shown in a series of subsequent discharges where the transitions from D^0 counter-NI to H^0 counter-NI, then to H^0 co-NI and, finally, to D^0 co-NI (P_{NI} = 0.9 MW) were performed for the same settings of the D^+ plasma. By taking into account the different power coupling for co- and counter-NI and for H^0 and D^0 injection, the confinement time for co-NI as well as for counter-NI prior to the onset of the profile peaking is 15 per cent higher when injecting D^0 instead of H^0 and the same increase is found when comparing the maximum confinement time of D^0 and H^0 counter-injection during the improved confinement phase. All these improved confinement regimes are characterized by radially peaked density profiles. The strongest peaking was achieved in deuterium plasmas fuelled with deuterium pellets (see Section 14).

In contrast, H-mode plasmas with broad density profiles also yield considerably improved confinement. The H-mode can be realized in hydrogen, deuterium, and in helium plasmas in ASDEX with either hydrogen or deuterium beams [26]. However, the accessibility of H-mode operation depends on the hydrogen isotope, the power threshold being a factor of 2 larger for hydrogen than for deuterium; this may be related to the higher edge temperature and hence larger edge pressure during the preceding L-mode phase in deuterium compared with hydrogen discharges. Simultaneously, the confinement time is higher for deuterium than for hydrogen in H-mode

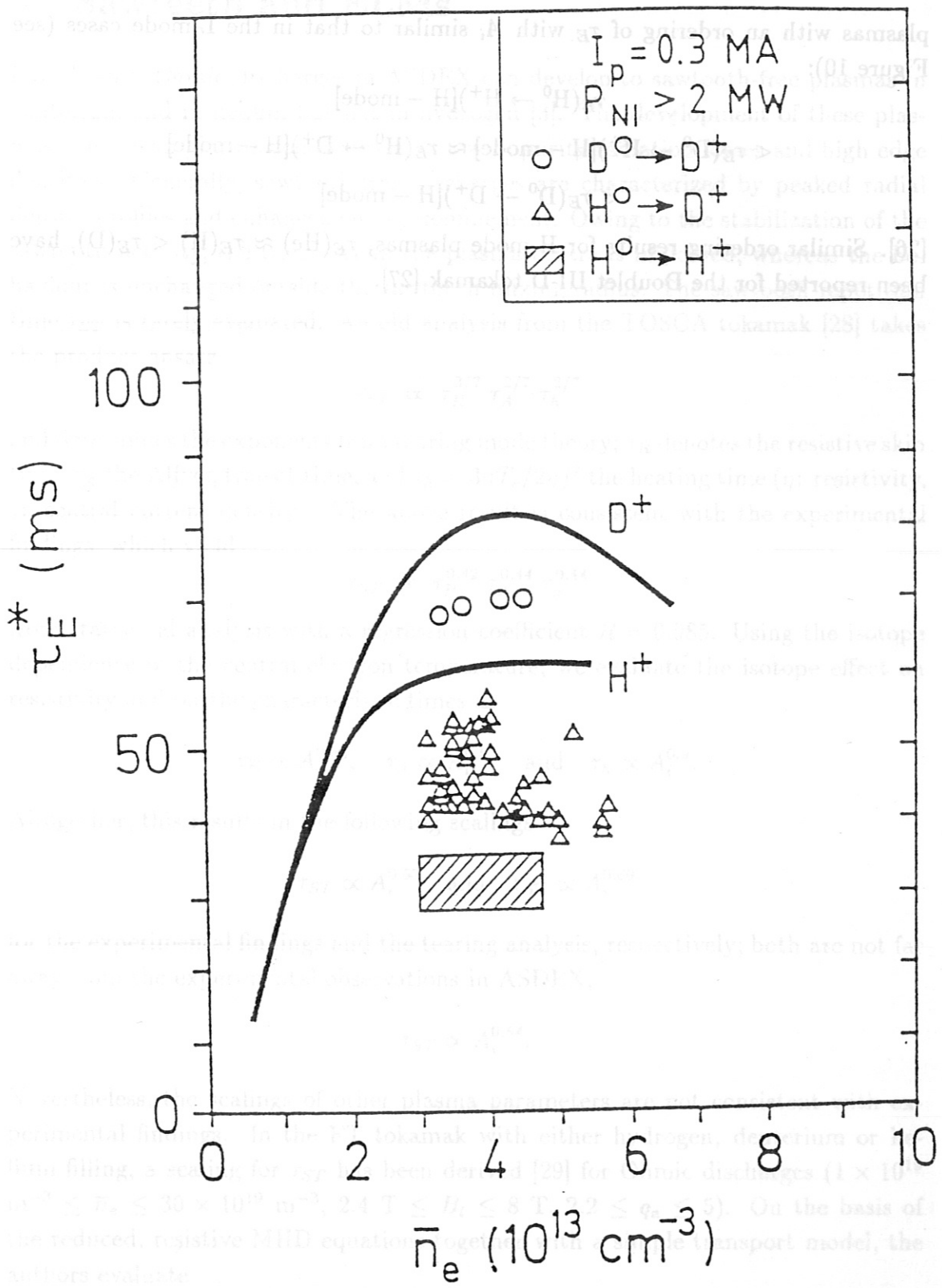

Figure 10: Energy confinement time as a function of electron density $\overline{n}_e$ for different H-mode scenarios, i.e. $H^0 \rightarrow H^+$, $H^0 \rightarrow D^+$, $D^0 \rightarrow D^+$. For comparison, the Ohmic data are included as fit curves [26].

plasmas with an ordering of τ_E with A_i similar to that in the L-mode cases (see Figure 10):

$$\tau_E(\mathrm{H}^0 \rightarrow \mathrm{H}^+)[\mathrm{H-mode}]$$
$$< \tau_E(\mathrm{D}^0 \rightarrow \mathrm{H}^+)[\mathrm{H-mode}] \approx \tau_E(\mathrm{H}^0 \rightarrow \mathrm{D}^+)[\mathrm{H-mode}]$$
$$< \tau_E(\mathrm{D}^0 \rightarrow \mathrm{D}^+)[\mathrm{H-mode}]$$

[26]. Similar ordering results for H-mode plasmas, $\tau_E(\mathrm{He}) \approx \tau_E(\mathrm{H}) < \tau_E(\mathrm{D})$, have been reported for the Doublet III-D tokamak [27].

5 Sawteeth and ELMs

Low-density *Ohmic* discharges in ASDEX can develop to sawtooth-free plasmas in deuterium and in helium but not in hydrogen [3]. The development of these plasmas need clean plasma conditions with low impurity radiation losses and high edge densities. Generally, sawtooth-free discharges are characterized by peaked radial density profiles and enhanced energy confinement. Owing to the stabilization of the sawtooth activity, the transport in the plasma centre is improved, whereas the behaviour is unchanged outside the sawtooth mixing radius. The sawtooth repetition time τ_{ST} is rarely evaluated. An old analysis from the TOSCA tokamak [28] takes the product ansatz

$$\tau_{ST} \propto \tau_R^{3/7} \tau_A^{2/7} \tau_h^{2/7}$$

and determines the exponents from tearing mode theory; τ_R denotes the resistive skin time, τ_A the Alfven transit time, and $\tau_h = 3nT_e/2\eta j^2$ the heating time (η: resistivity, j: central current density). The above result is consistent with the experimental findings, which yield

$$\tau_{ST} \propto \tau_R^{0.42} \tau_A^{0.44} \tau_h^{0.44}$$

from statistical analysis with a regression coefficient $R = 0.985$. Using the isotope dependence of the central electron temperature, we evaluate the isotope effect on resistivity and on the characteristic times as

$$\tau_R \propto A_i^{0.54}, \quad \tau_A \propto A_i^{0.5}, \quad \text{and} \quad \tau_h \propto A_i^{0.9}.$$

Altogether, this results in the following scalings

$$\tau_{ST} \propto A_i^{0.63} \quad \text{and} \quad \tau_{ST} \propto A_i^{0.69}$$

for the experimental findings and the tearing analysis, respectively; both are not far away from the experimental observations in ASDEX,

$$\tau_{ST} \propto A_i^{0.54}.$$

Nevertheless, the scalings of other plasma parameters are not consistent with experimental findings. In the FT tokamak with either hydrogen, deuterium or helium filling, a scaling for τ_{ST} has been derived [29] for Ohmic discharges (1×10^{19} m$^{-3} \leq \overline{n}_e \leq 30 \times 10^{19}$ m^{-3}, 2.4 T $\leq B_t \leq$ 8 T, $2.2 \leq q_a \leq 5$). On the basis of the reduced, resistive MHD equations together with a simple transport model, the authors evaluate

$$\tau_{ST} \propto \tau_E^{0.57} \times \Lambda_{Z_{\text{eff}}}^{0.18} \times A_i^{0.125}$$

where $\Lambda_{Z_{\rm eff}} = (3.4/Z_{\rm eff})\,((1.13 + Z_{\rm eff})\,/\,(2.67 + Z_{\rm eff}))$ being the $Z_{\rm eff}$-dependence of the resistivity. Applied to the isotope effect, the formula predicts

$$\tau_{ST} \propto A_i^{0.25} \quad \text{or} \quad A_i^{0.35}$$

for carbonized Ohmic ASDEX discharges in LOC or SOC, where $\tau_E \propto A_i^{0.31}$ or $\tau_E \propto A_i^{0.50}$ has been used (see Table 1). The predictions agrees quite well with the empirical result

$$\tau_{ST} \propto A_i^{0.25} \quad \text{or} \quad A_i^{0.54}$$

given in Table 1.

Like in the Ohmic case, the sawtooth behaviour under *L-mode* conditions in ASDEX is also rather different for the hydrogen isotope species [30]. For $H^0 \rightarrow D^+$, the repetition time τ_{ST} shows a sharp increase above 2 MW heating power at the L-H transition, whereas for $H^0 \rightarrow H^+$ this increase remains modest. Both in Ohmic and beam heating conditions, the sawtooth repetition time is larger in deuterium than in hydrogen plasmas. Therefore, we do not see any evidence for fast particle stabilisation of sawteeth as has been speculated by [31].

Without specific operational measures, *H-mode* plasmas in ASDEX are accompanied by *ELM* activity and it is observed that the ELM activity, namely the repetition rate, increases when going from deuterium to hydrogen plasmas; the same behaviour is reported from Doublet III-D. In addition, this behaviour depends on the heating power: At heating powers close to but still above the threshold for the L-H transition, the ELM behaviour is erratic with a high repetition rate known as grassy ELMs. With a further increase of the heating power, the ELM frequency decreases until, at sufficient heating power and after careful positioning of the plasma column inside the vessel, an ELM-free H*-mode can be reached provided the isotope mix is correct: With $H^0 \rightarrow H^+$, the quiescent H*-mode was never achieved. With $H^0 \rightarrow D^+$, it is possible to get an ELM-free H*-mode. With $D^0 \rightarrow D^+$, the H*-mode is achieved at lower heating power than in the mixed case. These ASDEX data indicate an ordering

$$\tau_E(H^0 \rightarrow D^+)[H-\text{mode}] < \tau_E(H^0 \rightarrow D^+)[H^*-\text{mode}] < \tau_E(D^0 \rightarrow D^+)[H^*-\text{mode}].$$

The use of deuterium instead of hydrogen seems to provide the same edge conditions as provided by higher power when the development of unstable edge conditions is slowed down. An explanation for this observation may be given by the ELM model described in [32]. In this model, resistivity plays a crucial role: Lower resistivity at the plasma edge tends to stabilize ELMs. In fact, higher edge temperatures are correlated with either the use of deuterium instead of hydrogen or the use of higher heating power. Hence, model and observations are in good agreement.

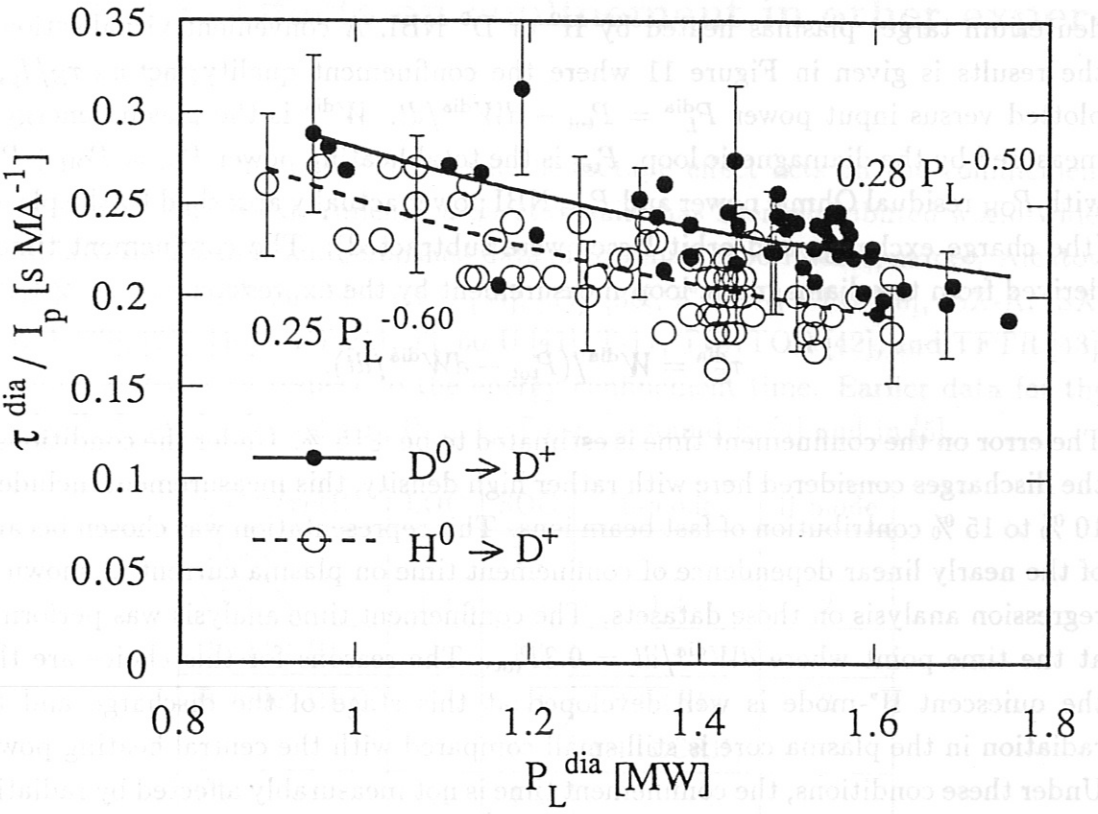

Figure 11: Isotope effect in H*-mode discharges. Quality factor $\tau_E^{\rm dia}/I_p$ versus input power $P_L^{\rm dia} = P_{\rm tot} - dW^{\rm dia}/dt$. The lines indicate the fit of a power dependence for both set of data. The operational window of the discharges was 0.22 MA $\leq I_p \leq$ 0.42 MA and 1.2 T $\leq B_t \leq$ 2.8 T, corresponding to $2.5 \leq q_a \leq 4$.

ELMs cause a rapid loss of energy and particles which is different from the loss between ELMs due to microscopic transport (see Section 15). Thus, the results of conventional transport analysis will be misleading if the ELM behaviour is ignored. It has been shown that the transport properties of ELMy H-mode discharges in the unaffected region equals that of ELM-free H*-mode if the energy loss owing to the ELMs is correctly taken into account [33]. This indicates that the intrinsic transport properties of the H-mode are the same in the two cases, although the uncorrected values of τ_E may differ by a factor of 1.5 to 2. The comparison of an H-mode with $H^0 \rightarrow H^+$ and high ELM frequency to a discharge with $D^0 \rightarrow D^+$ and only few ELMs without any ELM correction will therefore lead to an overestimate of the isotope effect on the intrinsic transport properties of the H-mode.

In addition, ELM-free H*-mode discharges serve to reveal the pure isotope effect on the H-mode confinement time. The available data allows the comparison of

deuterium target plasmas heated by H^0 or D^0 NBI. A convenient visualisation of the results is given in Figure 11 where the confinement quality factor, τ_E/I_p, is plotted versus input power $P_L^{\mathrm{dia}} = P_{\mathrm{tot}} - dW^{\mathrm{dia}}/dt$. W^{dia} is the plasma energy as measured by the diamagnetic loop, P_{tot} is the total heating power $P_{\mathrm{tot}} = P_{\mathrm{OH}} + P_{\mathrm{abs}}$, with P_{OH} residual Ohmic power and P_{abs} NBI power actually absorbed by the plasma (the charge exchange and orbit losses were subtracted). The confinement time is derived from the diamagnetic loop measurement by the expression

$$\tau_E^{\mathrm{dia}} = W^{\mathrm{dia}}/(P_{\mathrm{tot}} - dW^{\mathrm{dia}}/dt).$$

The error on the confinement time is estimated to be ±15 %. Under the conditions of the discharges considered here with rather high density, this measurement includes a 10 % to 15 % contribution of fast beam ions. This representation was chosen because of the nearly linear dependence of confinement time on plasma current as shown by regression analysis on these datasets. The confinement time analysis was performed at the time point where $dW^{\mathrm{dia}}/dt = 0.3P_{\mathrm{tot}}$. The reasons for this choice are that the quiescent H*-mode is well developed at this stage of the discharge and the radiation in the plasma core is still small compared with the central heating power. Under these conditions, the confinement time is not measurably affected by radiation losses and the dataset is as homogeneous as possible. Moreover, the confinement time is measured well before the discharges reach the beta limit. These important conditions would not be fulfilled if the analysis were made at the maximum of the plasma energy.

The hydrogen concentration in the $H^0 \rightarrow D^+$ discharges is not known, but Figure 11 qualitatively shows that the isotope mass also influences the intrinsic H-mode confinement, in a way similar to what is observed in the other regimes. If we assume that there is a 50 % mix of hydrogen and deuterium in the H^0 injection case and a 100 % clean deuterium plasma in the D^0 injection case, the measured ratio of $\tau_E(H^0 \rightarrow D^+)/\tau_E(D^0 \rightarrow D^+)$ gives a scaling $\tau_E \propto A_i^{0.46}$, which agrees with the L-mode results. The somewhat stronger power degradation for H^0 injection is internally consistent with the isotope effect because increasing power corresponds to an increased hydrogen concentration.

6 Isotope effects on confinement in other experiments

To clarify whether and to what extent the isotope effect acts on the confinement times of other fusion experiments, a questionnaire has been distributed world-wide. In Table 3, the answers and published data of tokamak experiments, namely Alcator, ASDEX, Doublet III, Doublet III-D [34]; [35]; [36], FT [37], FTU [38], ISX-A, ISX-B, JET [39]; [31]; [40], JFT-2M, JT-60 U [41], T-11, TEXTOR [42], and TFTR [43], are summarized with respect to the energy confinement time. Earlier data for the Ohmically heated tokamaks TFR and ST can be found in [4] and in [5].

$\tau_E(D)/\tau_E(H)$	LOC	SOC	L-mode	H-mode
Alcator		1.5		
ASDEX	1.3	1.5	1.4	2
Doublet III	1	1.4	1.4	
Doublet III-D		1.4	1.0 (NI) 1.4 (ECRH)	2
FT	1.1	1.5		
FTU	1.1	1.4		
ISX-A	1.4	1.4		
ISX-B	1.4	1.4		
JET		1.4	1.2	
JFT-2M	1.1	1.4	1.4	1.4
JT-60 U	1.2		1.4–1.6	
T-11	1.3			
TEXTOR	1.4	1.4		
TFTR			1.15	

Table 3: Ratio of $\tau_E(D)/\tau_E(H)$ as reported for various experiments from the world-wide questionnaire.

Evidently, the isotope effect on τ_E appears in nearly all tokamaks and in different confinement scenarios, ranging from low-density Ohmic (LOC), high-density Ohmic (SOC), L-mode up to H-mode discharges with roughly the same factor $\tau_E(D)/\tau_E(H)$ around $\sqrt{A_i}$. There is a general trend that the isotope effects decrease with the size of the tokamak.

An important aspect is the lack of any isotope effect in the case of Doublet III-D

in the L-mode with neutral injection. On the other hand, an isotope effect has been observed in the L-mode of Doublet and it is also present in Doublet III-D under Ohmic heating and with electron cyclotron resonance heating. Unlike the reduction of the isotope effect toward higher power is understandable, its complete lack is of importance. It may imply that the isotope effect is *not* an *intrinsic* property of the heat diffusivities but it is introduced by an external property, generally realized but not on Doublet III-D with neutral injection under L-mode conditions, although it clearly appears with beam injection into H-mode plasmas [35]; [34]. The contribution of ASDEX to the question of the A_i scaling being an intrinsic property or externally introduced will be presented below.

The two largest machines, JET and TFTR, behave quite similar: In JET, a relation $\tau_E \propto A_i^{0.56}$ is stated for Ohmic conditions [39]; for L-mode conditions, an average improvement of 15 per cent is observed for τ_E [31]. In TFTR, hydrogen plasmas are also worse in energy confinement than deuterium plasmas. Ohmic confinement data are consistent with the ASDEX power flux model [44], but the isotope effect is relatively small in L-mode with $\tau_E \propto A_i^{0.2\pm0.1}$ [43] like in JET. One reason may be that TFTR isotope studies choose roughly equal radial density profiles for both hydrogen isotopes and compare mainly plasmas with similar deuterium neutral-beam-heating power in the intention to keep beam effects also the same. Local transport coefficients and radiative losses are then roughly equal [45]. The momentum confinement time as well as the sawtooth repetition time and the recycling light in the edge seem not to scale with species mass in TFTR. These data indicate the expectation that the isotope effect in L-mode plasmas follows primarily as a consequence of the collisionality which is of minor importance in the larger tokamak machines such that they show smaller isotope effects. Another plausible explanation may be that transport in the smaller machines may be dominated by electrons whereas in the larger machines ion-dominated transport is likely to occur.

In recent TEXTOR I-mode discharges, isotopic effects show up as a 35 % ($\tau_E \propto A_i^{0.43}$) increase in τ_E of $D^0 \rightarrow D^+$ discharges over $H^0 \rightarrow H^+$ discharges, a 17 % ($T_{e0} \propto A_i^{0.23}$) increase in T_{e0}, and roughly the same density peaking factor [46].

As a consequence of the isotopic dependence of τ_E in various tokamaks, the H-mode database working group includes the isotope composition in its standard dataset [47]. The group analyzed the energy confinement in six tokamaks, namely ASDEX, D III-D, JET, JFT-2M, PBX-M, and PDX, and extracts recently thermal scalings for ELMy data

$$\tau_{E,th} = 0.034 I_p^{0.90} \times B_t^{0.05} \times P_{in}^{-0.65} \times A_i^{0.40} \times R^{2.1} \times \kappa^{0.80} \times (a/R)^{0.20} \times \overline{n}_e^{0.30}$$

with $P_{in} = P_{heat} - P_{loss} - dW_{tot}/dt$ and ELM-free data

$$\tau_{E,th} = 0.032 I_p^{0.95} \times B_t^{0.20} \times P_{in}^{-0.65} \times A_i^{0.45} \times R^{1.95} \times \kappa^{0.65} \times (a/R)^{0.05} \times \overline{n}_e^{0.30}$$

where the units are (s; MA, T, MW, ., m, ., ., 10^{19} m^{-3}). Both scalings show indeed a strong isotope effect on energy confinement with the interesting observation that the effective isotope exponent is not a constant but increases with $P_{in}/\overline{n}_e V$, i.e. the mean energy per particle, from the lowest value in JET up to the ASDEX value.

The survey on the isotopic behaviour in experiments other than ASDEX addressed also the particle confinement. The particle confinement time τ_p is found to be even more influenced by the ion species than τ_E: $\tau_p(D)/\tau_p(H) \approx 1.5$ to 2 in ASDEX. Similar factors are found for example in the TEXTOR limiter tokamak [42] and in the JET L-mode plasmas [31].

The survey tries also to compare the confinement of helium discharges compared with hydrogen or deuterium plasmas (see Section 13). Here, a broad spectrum of $\tau_E(He)/\tau_E(H)$ values is observed, ranging from 0.8 for JFT-2M to 1.5 for ASDEX conditions.

Little is known about the isotope effect in stellarators [48]. ATF reports that there is no isotope effect [49]. The regression analysis of the ATF data base yields $\tau_E \propto A_i^{-0.2}$. This scaling fits well to the expectation of neo-classical theory or simple drift wave models with a $\chi \propto A_i^{-0.5}$. On Wendelstein VII-AS, isotope studies are still preliminary. Data which were obtained from a sequence of discharges where the gas was changed from hydrogen to deuterium did not indicate an isotope dependence of τ_E after correction for the slightly different density and ECR heating power in the two sets. More has to be done in the future to clearly answer the existence or non-existence of an isotope effect on the confinement of stellarators.

7 Evidence for the isotope effect in the build-up phase of a discharge

ASDEX experiments clearly reveal that the isotope effect is already present during the plasma build-up as well as the discharge ramp-down phases, where the current profile is not steady state, the divertor configuration is not yet well established, and the electron distribution may deviate from a Maxwellian.

During the ramp-up phase, 50 ms after discharge initiation, the isotope effect shows up in the gas consumption and in the ratio H_α/D_α in the main plasma of the discharge, being less in deuterium than in hydrogen. Differences in gas consumption and in H_α/D_α indicate the appearance of the isotope effect in particle confinement under still non-thermal plasma conditions. Later, after 150 – 200 ms, differences in $\beta_{\rm pol}^{\rm dia}$ and in the central electron temperature, as given by electron cyclotron emission traces, also indicate the appearance of the isotope effect on energy transport. The discharge current is developed typically after 500 ms and the density built-up is completed after 600 ms. The comparison of this phase with the divergence in the ratio H_α/D_α between hydrogen and deuterium discharges clearly shows that the isotope effect on particle confinement is always present under still non-thermal plasma conditions.

To study the impact of the plasma breakdown condition on the isotope effect, we compared two discharges of identical initial phases. In both cases, the plasma breakdown and the current ramp-up phase was done in helium. Till the current plateau phase was reached, the density was kept low at $\overline{n}_e = 1.5 \times 10^{19}$ m^{-3}. In the current plateau phase the density was ramped up to $\overline{n}_e = 4.5 \times 10^{19}$ m^{-3} in one case by hydrogen and in the other case by deuterium gas puffing. The idea behind this study was to assess whether the larger gas consumption of a hydrogen plasma during the density ramp-up phase has a deleterious impact on the confinement in the plateau phase. This could have been expected because the larger gas supply during the ramp-up phase of the discharge will be recycled during the plateau phase. There are many cases where larger external gas flux is linked to lower particle and energy confinement. No effect, however, was detected during the plateau phases which displayed the usual differences between hydrogen and deuterium. Obviously, it is not the start-up condition which causes the isotope effect as observed under plateau conditions.

8 Isotope effect close to the density limit

Supplementary to these early phases of tokamak discharges, high-density plasmas ($\overline{n}_e = 5.4 \times 10^{19}$ m^{-3}, $I_p = 320$ kA, $B_t = 2.2$ T, $q_a = 3.3$) have been investigated for hydrogen, deuterium and helium in order to study the isotope effect close to the density limit under cold and highly collisional conditions. These plasmas are characterized by 490, 420 and 420 kW Ohmic heating power and 100, 130, 130 kW total radiation power loss (mostly oxygen lines) in the bulk, respectively. The Murakami parameter is $M = 4 \times 10^{19}$ m^{-2} T^{-1}; the density limit is reached for these plasmas at $M = 5 \times 10^{19}$ m^{-2} T^{-1}. The power flux into the SOL is comparable for deuterium and helium but significantly higher for hydrogen as given in Figure 12. Accordingly, the net power load onto the divertor plates, which is integrated over the whole discharge with the help of calorimeters, sums up to 231, 139, and 144 kJ, respectively, which reflects the unfavourable target load condition of the hydrogen case.

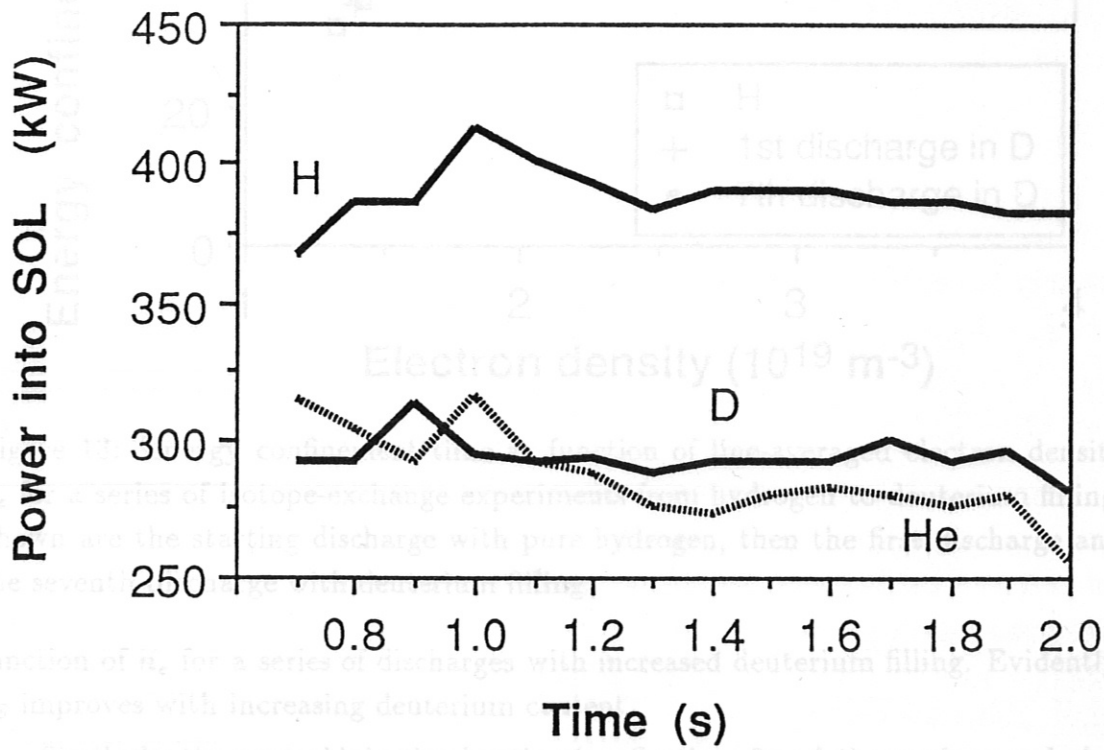

Figure 12: Power flux into the SOL for high-density discharges ($I_p = 320$ kA, $B_t = 2.2$ T, $\overline{n}_e = 5.4 \times 10^{19}$ m^{-3}) with either hydrogen, deuterium or helium filling under boronized wall conditions.

No significant isotope effect, however, in the density limit is observed on ASDEX

[15], whereas helium plasmas exceed the density limit of deuterium by almost a factor of 2. Nevertheless, a common *edge* density limit is observed.

9 The role of the effective ion mass

From the above observations it is obvious that the isotope effect is of an *additive* nature. Relevant for confinement is the mean plasma mass A_{eff}, ranging between 1 and 2. Figure 13 shows the result of a hydrogen to deuterium gas exchange fuelling experiment under Ohmic conditions. The energy confinement time is sketched as a

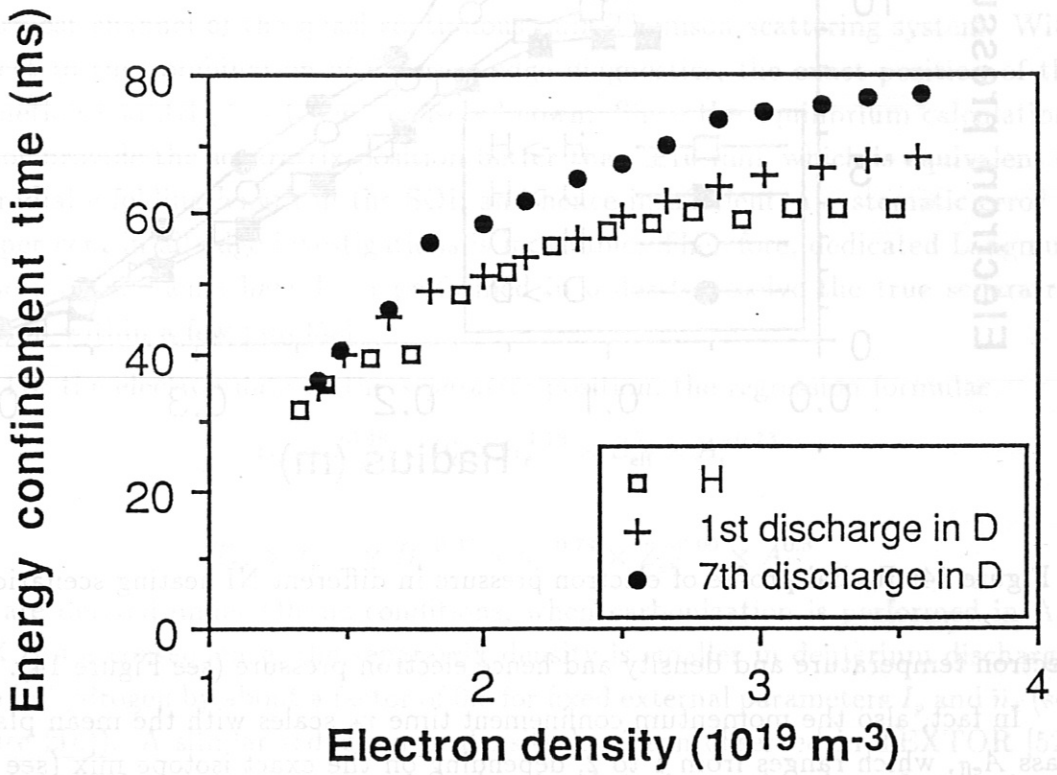

Figure 13: Energy confinement time as function of line-averaged electron density $\overline{n}_e$ for a series of isotope-exchange experiments from hydrogen to deuterium filling. Shown are the starting discharge with pure hydrogen, then the first discharge and the seventh discharge with deuterium filling.

function of $\overline{n}_e$ for a series of discharges with increased deuterium filling. Evidently, τ_E improves with increasing deuterium content.

Similarly, the neutral injection heating (see Sections 3 and 4) reveals an ordering of the form

$$\tau_E(\mathrm{H}^0 \rightarrow \mathrm{H}^+) < \tau_E(\mathrm{D}^0 \rightarrow \mathrm{H}^+) \approx \tau_E(\mathrm{H}^0 \rightarrow \mathrm{D}^+) < \tau_E(\mathrm{D}^0 \rightarrow \mathrm{D}^+)$$

for both L-mode and H-mode scenarios which is illustrated by Figure 7. This confinement behaviour is accompagnied by a similar ordering of the radial profiles of

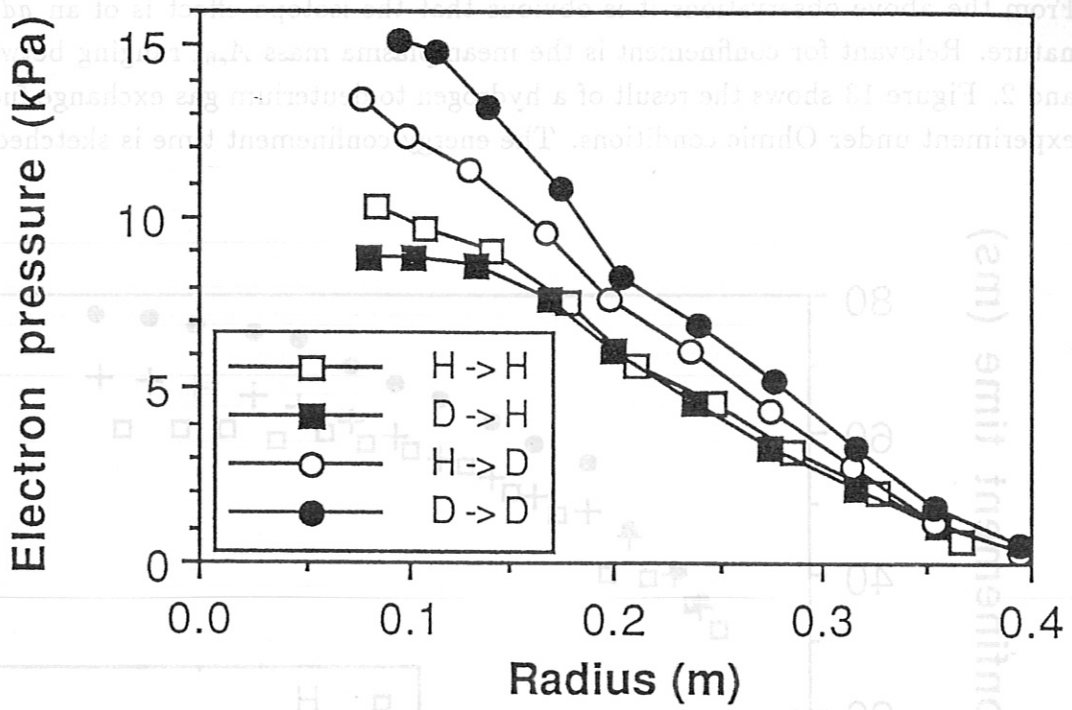

Figure 14: Radial profile of electron pressure in different NI heating scenarios.

electron temperature and density and hence electron pressure (see Figure 14).

In fact, also the momentum confinement time τ_Φ scales with the mean plasma mass A_{eff}, which ranges from 1 to 2, depending on the exact isotope mix (see Section 11).

10 Edge and divertor effects

The Scrape-Off Layer (SOL) and divertor plasmas show pronounced isotope effects. At the separatrix position, the electron density and temperature are measured here with a five-point Thomson scattering system of high resolution and sensitivity and with Langmuir probes. In addition, a thermal lithium atomic beam is used to resolve the relative density profile. These items of information are linked to the outermost channel of the quasi-continuous bulk Thomson scattering system. With respect to the combination of different edge diagnostics, the exact position of the magnetic separatrix has to be precisely known. Since the equilibrium calculations do not provide the separatrix position better than ± 10 mm, which is equivalent to the radial e-folding length in the SOL and hence insufficient, a systematic error of 100 per cent in all edge investigations is inevitable. Therefore, dedicated Langmuir probe measurements have been performed in order to resolve the true separatrix position within a few mm [50].

For the electron data at the *separatrix* position, the regression formulae

$$n_{es} \propto I_p^{0.48} \times B_t^0 \times \overline{n}_e^{1.18} \times Z_{\mathrm{eff}}^0 \times A_i^{-0.73}$$

and

$$T_{es} \propto I_p^{1.27} \times B_t^{-0.37} \times \overline{n}_e^{-0.74} \times Z_{\mathrm{eff}}^{-0.09} \times A_i^{0.3}$$

[51] are derived under Ohmic conditions, when carbonization is performed in ASDEX. As a consequence, the separatrix density is smaller in deuterium discharges than in hydrogen by about a factor of 0.6 for fixed external parameters I_p and $\overline{n}_e$ (see Figure 2(c)). A similar reduction in density has been observed in TEXTOR [52]. The separatrix temperature, on the other hand, is detected to be a factor of 1.28 higher in deuterium than in hydrogen for fixed I_p, B_t, and Z_{eff} in ASDEX. Nevertheless, a slower thermal velocity for deuterium compared with hydrogen comes up and hence a shorter penetration depth. The temperature result differs from TEXTOR results [42] where the electron temperature at the limiter ($a = 0.46$ m) is seen to be smaller by a factor of 0.6 with deuterium fuelling compared with hydrogen fuelling. The ion temperature of C^{6+} at the TEXTOR limiter is reduced even by a rough factor of four in deuterium discharges compared to hydrogen discharges [53]. Nevertheless, the difference between data of hydrogen and deuterium plasmas vanish at some distance ($r/a = 0.85$) from the limiter.

Concerning different wall conditioning procedures, it has to be noticed that the isotope scalings in the edge plasma fade away when going from carbonization to boronization. The regression analysis of the Ohmic data base yields

$$n_{es} \propto I_p^{0.24} \times B_t^{0.17} \times \overline{n}_e^{1.11} \times Z_{\mathrm{eff}}^0 \times A_i^{-0.32}$$

and

$$T_{es} \propto I_p^{1.16} \times B_t^0 \times \overline{n}_e^{-0.52} \times Z_{\rm eff}^0 \times A_i^0$$

[51], which indeed expresses a weaker isotope effect after boronization than after carbonization (see above). These observations may be related to increasing cleanliness with reduced $Z_{\rm eff}$ and therefore similar $P_{\rm sol}$.

Detailed regression analysis in ASDEX [54] for the radial e-folding length λ_n of the density profile in the SOL yields

$$\lambda_n = \lambda\, q_a^{\alpha},$$

with λ and α both being weakly sensitive to the isotope mass, i.e. λ(H) = 11.8 mm, λ(D) = 12.9 mm, λ(He) = 13.2 mm and α(H) = 0.4, α(D)=0.35 and α(He) = 0.52 close to 0.5. Thus, λ_n follows mainly a $q_a^{1/2}$-dependence with only minor isotopic contributions. These observations are supported by a rough estimate of λ_n from anomalous radial transport, characterized by the diffusion coefficient $D^{(\rm an)}$ and the convective velocity $v^{(\rm an)}$. To this aim, the continuity equation in the stationary state

$$D^{(\rm an)} n_e'' - v^{(\rm an)} n_e' \approx n_e v_{\|} / L_c$$

is solved for the exponential decaying density profile

$$n_e = n_{es} \exp\{-(r - r_s)/\lambda_n\}$$

in the SOL ($r \geq r_s$), where $'$ denotes the radial derivative, L_c the connection length and $v_{\|}$ the parallel velocity. We obtain

$$\lambda_n = (\lambda_d^2/\lambda)\,(1 + \{1 + (\lambda/\lambda_d)^2\}^{1/2}),$$

with $\lambda_d = \{D^{(\rm an)} L_c / v_{\|}\}^{1/2}$ being the diffusion dominated length and $\lambda = 2D^{(\rm an)}/v^{(\rm an)}$ the profile width. Normally, it is $\lambda \gg \lambda_d$; thus,

$$\lambda_n \approx \lambda_d \{1 + (\lambda_d/\lambda)\}.$$

Taking $D^{(\rm an)}$ and $v^{(\rm an)}$ from the measurements (see Section 11), we can calculate the isotope scaling of λ_n. The results agree well with the regression analysis data given above in both, showing mainly the $q_a^{1/2}$-dependence and a weak isotope dependent factor.

In fact, the neutral mean free path λ_0 in the SOL plasma, i.e. the neutral penetration, is also different for the hydrogen isotopes. Since the neutrals suffer both charge exchange and ionization collisions, the effective penetration has to be

calculated from kinetic equations including inhomogeneous temperature and density profiles in the edge. The result, as given by [55], is

$$\lambda_0 \propto n^{-1} T_i^{1/2} A_i^{-1/2};$$

for illustration, it is

$$\lambda_0(\mathrm{He}) : \lambda_0(\mathrm{H}) : \lambda_0(\mathrm{D}) = 1.3 : 1.0 : 0.71$$

for constant density and temperature profiles and $L = 2\lambda_T/\lambda_0 = 3$.

With respect to *divertor* data, it has to be noted that several changes werde made in the divertor configuration during the ten years of ASDEX operation. The early version (DV-I) was characterized by titanium divertor plates, large divertor volume and low vacuum conductance between divertor and main chamber. In order to withstand higher divertor heat load, the water-cooled configuration (DV-II) was designed [56] which has copper divertor plates, small divertor volume and relatively high vacuum conductance between divertor and main chamber. Therefore the gas consumption of DV-II is lower by a factor of 2 and the neutral gas pressure, measured in the outer divertor reservoir is reduced [57]. This results in different recycling behaviour of DV-I and DV-II. In both divertor configurations, the electron data as obtained by triple probes follow the general trends of the separatrix data in the main chamber: The electron temperature T_{ed} remains about the same for hydrogen and deuterium, whereas the electron density n_{ed} in deuterium is half the value of n_{ed} in hydrogen discharges [44]. With boronized walls, this difference in n_{ed} reduces to a factor of 1.5 between hydrogen and deuterium similar to the reduced isotope effect on n_{es}. The density behaviour is further verified by microwave interferometry; a typical example is shown in Figure 15 for high-density ($\overline{n}_e = 5.4 \times 10^{19}$ m^{-3}) discharges in hydrogen or deuterium. This behaviour is well correlated with the enhanced particle confinement in deuterium discharges. In addition, measurements by ionization gauges reveal the neutral density to be a factor of 2 larger for hydrogen than for deuterium in the divertor chamber. Concerning the discharges with three density plateaus ($\overline{n}_e = 2.5$, 4.0 and 5.5×10^{19} m^{-3}, $I_p = 380$ kA, $B_t = 2.2$ T, $q_a = 2.8$) for either hydrogen or deuterium filling an increase of the divertor radiation is observed, as obtained from bolometry. With increasing density, the divertor radiation reaches a level of 45 per cent of Ohmic heating for deuterium and of 55 per cent for hydrogen. The sum of main plasma radiation and divertor radiation is about 70 per cent of the Ohmic heating for both hydrogen isotopes. The missing power may be attributed to charge-exchange losses in the X-point region or to radiation in the divertor throats which are not accessible to the measurements.

Concerning impurity release, it has to be considered that, owing to its heavier mass, the deuterium particle can sputter more strongly than the hydrogen particle

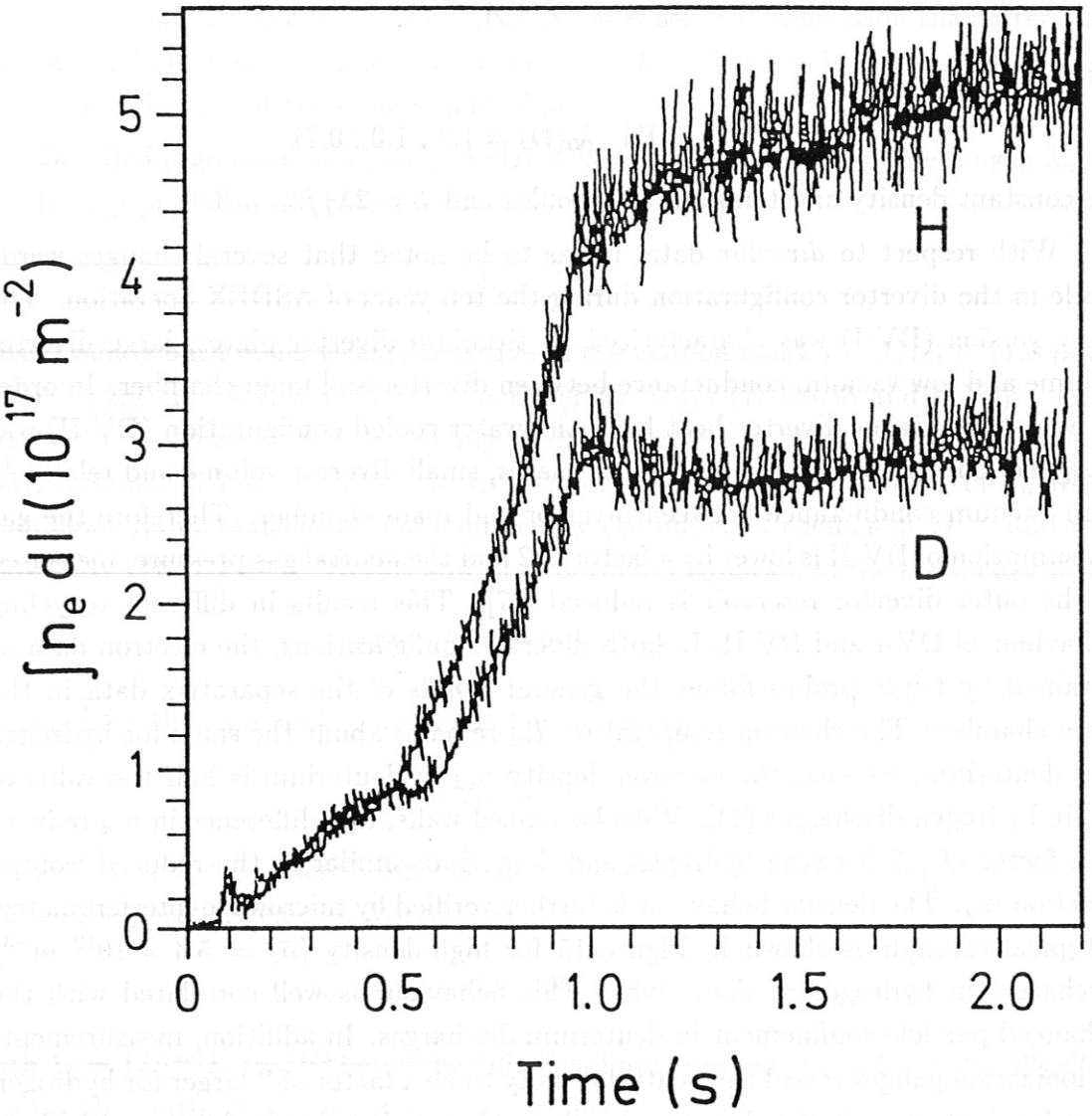

Figure 15: Line-integrated electron densities in the divertor chamber as determined by microwave interferometry for high density discharges ($I_p = 320$ kA, $B_t = 2.2$ T, $\overline{n}_e = 5.4 \times 10^{19}$ m^{-3}) with either hydrogen(#28640) or deuterium(#28813) filling.

under the same plasma conditions. For standard ASDEX discharges with a divertor temperature of 10-20 eV, the increase is by an order of magnitude. In order to calculate impurity fluxes, this erosion yield has to be multiplied by the particle flux, which also depends on the plasma mass: Since the electron density in the divertor DV-II is roughly twice as large for H^+ as for D^+ at the same bulk density, whereas the divertor temperature seems to be rather independent of A_i, the resulting sputtered impurity (here: copper) fluxes are only a factor of 2 to 3 lower for H^+ than for D^+. These evaluations are confirmed by spectroscopic measurements of the copper fluxes in the divertor chamber [58]. Furthermore, the ASDEX results indicate that the copper flux from the divertor plates is increased with additional heating via neutral injection and shows no isotope dependence any more for high densities, i.e. H^+ and D^+ release roughly the same amount of impurity fluxes, since the divertor power loads are then roughly the same. The iron influx from the wall into ASDEX divertor DV-I plasmas, however, has been determined spectroscopically to be a factor of 6 higher in deuterium than in hydrogen. This can readily be explained by enhanced sputtering due to the larger flux of charge-exchange neutrals, as measured by the CX time-of-flight analyzer (see Section 11), together with improved impurity confinement [59]. Since $n_{es}(\mathrm{D}) < n_{es}(\mathrm{H})$ holds, the CX particles stem from deeper zones inside the bulk plasma in the case of deuterium and hence have larger temperature which also leads to enhanced sputtering rates. A similar isotope dependence is observed spectroscopically in ISX-B [16], where the Fe IX concentrations, coming mainly from the wall, were determined to be a factor of 3 higher in deuterium than in hydrogen discharges, this being consistent with CX sputtering as erosion mechanism, too.

In order to quantify things, an analytical model solves the one-dimensional heat conductivity equation along field lines in the SOL ([60]; [61]; [62]; [18]). As a boundary condition at the separatrix in the midplane, the net power input $P_{\mathrm{sol}} = P_{\mathrm{tot}} - P_{\mathrm{rad,main}}$ into the SOL is included, which describes the reduction of the total power input P_{tot} by radiation $P_{\mathrm{rad,main}}$ in the bulk and in the boundary plasma. At the divertor plates, the power is deposited ($\delta n_{ed} k_B T_{ed} v_{\|}$ with sheath energy transfer factor δ [63]) or used to ionize neutral particles by stepwise ionization processes ($n_{ed} E_{\mathrm{ion}} v_{\|}$ with average energy loss E_{ion} per ionization event) or radiated away ($P_{\mathrm{rad,div}}$). Altogether, the solution for the temperature distribution reads

$$T_{es}^{7/2} = T_{ed}^{7/2} + (7/2)(P_{\mathrm{sol}}/A_{\mathrm{sol}}) L_c/\kappa_0$$

along the connection length L_c, with $\kappa_{\|} = \kappa_0 T_e^{5/2}$ taken from Spitzer's law and the effective SOL surface $A_{\mathrm{sol}} = 2\pi R \lambda_P B_t/B_p$ (λ_P : effective power channel width). Provided the net power influx P_{sol} into the SOL and one of the temperatures (T_{es} or T_{ed}) are known, the other temperature (T_{ed} or T_{es}) may be estimated. To calculate

the separatrix density, the momentum balance equation is solved along field lines with Mach numbers $M = 0$ at the separatrix and $M = 1$ at the divertor sheath. With all pieces put together, the separatrix density n_{es} is determined by

$$n_{es} T_{es} T_{ed}^{1/2} (1 + (E_{\rm ion}/\delta k_B T_{ed})) = (2\pi m_i/k_B^3)^{1/2} 2 P_{\rm div}/(A_{\rm sol}\delta)$$

with $P_{\rm div} = P_{\rm sol} - P_{\rm rad,div}$. In this framework, the ion temperature T_i has not necessarily to be equal to the electron temperature T_e. Even a ratio $T_i/T_e \approx 5$ would imply a mere 10 per cent change of the rhs of the above equation. Since $A_{\rm sol}$ is proportional to the effective power channel width λ_P, which increases at least linearly with q_a in the range $q_a = 2.5$ to 5 [15], it seems that even this simple model can predict the right q_a-dependence in the density limit.

With regard to the isotope effect, the separatrix correlation

$$T_{es} \propto n_{es}^{-2/3} \times P_{\rm div}^{2/3} \times A_i^{1/3}$$

follows if the density is low enough such that $E_{\rm ion} \ll \delta k_B T_{ed}$ holds and the power channel width λ_P is only weakly affected by the isotope mix as it is the case for λ_n. The above model relation agrees quite well with the empirical three-parameter regression formula

$$T_{es} = 92\, n_{es}^{-0.77} \times P_{\rm sol}^{0.65} \times A_i^{0.2} \qquad ({\rm eV}, 10^{19}{\rm m}^{-3}, {\rm MW})$$

obtained from the Ohmic data base with a regression coefficient $R = 0.94$. Intuitively, these results reveal that the edge physics in the SOL remains about the same. There is only a weak explicit isotope dependence detectable. However, the separatrix temperature also implicitly depends on the isotope mass via the different energy influxes into the SOL. Since Ohmic heating power is higher for hydrogen compared with deuterium (owing to the lower central electron temperature which offsets the lower $Z_{\rm eff}$) and the radiation losses are lower for hydrogen than for deuterium, the net power influx into the SOL is appreciably smaller for deuterium than for hydrogen (see Section 2). As the reduced power flux goes along with reduced desorption, actually the separatrix density is decreased, whereas the separatrix temperature is only slightly modified. The low separatrix density and high separatrix temperature seem to be favourable boundary conditions with respect to bulk confinement. As to the isotope dependences of the edge parameters themselves under these low density conditions, the model evaluates

$$T_{es} \propto A_i^{0.32}, \quad n_{es} \propto A_i^{-0.78}, \quad \text{and} \quad n_{ed} \propto A_i^{-0.84}$$

if the isotope effects on the power loads $P_{\rm sol}$ and $P_{\rm div}$ and on T_{ed} are given as input and the external parameters I_p, B_t, and $\overline{n}_e$ are kept constant. These calculated scalings lie close to the experimental observations given above.

Finally, the effects of wall conditioning will be addressed. From carbonized wall conditions to boronized ones, the impurity content and consequently the radiation losses drop. For deuterium, the ratio of radiated to Ohmic power, for example, decreases from 45 per cent under carbonized conditions to 25 per cent under boronized ones. Therefore, the values of the power input into the SOL of hydrogen and deuterium plasmas approach each other. Accordingly, the theoretical model predicts a weaker isotope scaling of the separatrix data with boronization than with carbonization. In fact, the corresponding scalings

$$T_{es} \propto A_i^{0.32}, \quad n_{es} \propto A_i^{-0.33}, \quad \text{and} \quad n_{ed} \propto A_i^{-0.40}$$

are derived for fixed external parameters which are also close to the observed regression data (see above).

To be on the safe side, the theoretical considerations are further extended to simulations of an Ohmic isotope scan in ASDEX which includes helium discharges (see Section 13). To this aim, the separatrix density is estimated from the separatrix correlation, i.e. n_{es} is determined as a function of the measured separatrix temperature T_{es} and the power influx P_{sol}, and compared with the measured density n_{es} in all three fuelling cases, namely for hydrogen, deuterium and helium. The results in terms of density ratios are

$$n_{es}(\mathrm{H})/n_{es}(\mathrm{D}) = 1.31, \qquad n_{es}(\mathrm{H})/n_{es}(\mathrm{He}) = 1.36, \qquad n_{es}(\mathrm{D})/n_{es}(\mathrm{He}) = 1.04,$$

which agree well with the measured ratios

$$n_{es}(\mathrm{H})/n_{es}(\mathrm{D}) = 1.28, \qquad n_{es}(\mathrm{H})/n_{es}(\mathrm{He}) = 1.39, \qquad n_{es}(\mathrm{D})/n_{es}(\mathrm{He}) = 1.09.$$

This makes us confident that the simple edge model comprises the main features of the edge isotope effect in ASDEX.

11 Particle confinement

With respect to *particle confinement*, the edge and divertor measurements as reported in Section 10 serve to evaluate the total particle flux Φ across the SOL surface into the bulk plasma. This flux splits up into a recycling part Φ_{recyc} and external fuelling Φ_{fuel}. In the stationary case, the total particle flux Φ across the last closed flux surface (LCFS) just balances the total particle loss N_p/τ_p within the LCFS, which determines the global particle confinement time

$$\tau_p = \Phi/N_p.$$

In addition, Φ gives rise to a convective energy flux

$$Q_{\text{conv},q} = (5/2)\,\Phi\,k_B T_{q,s}$$

for each particle species q ($q = e$ or $q = i$). Fluctuation studied at the plasma edge indicate that this convective term normally represents the dominant energy loss into the boundary plasma of a tokamak, not only in a divertor tokamak such as ASDEX but also in a limiter tokamak such as TEXT [64]. With respect to the isotope effect, the hydrogen particle flux Φ is observed to be typically twice as large as the deuterium flux for otherwise equal discharge conditions. This agrees with the higher separatrix density for hydrogen compared with deuterium, since the particle flux increases approximately proportionally to the separatrix density. This behaviour is also consistent within the framework of electrostatic turbulence [65]. It is also not surprising that the isotopic difference in particle flux decreases with enhanced wall conditioning via boronization as a consequence of the increased power flux into the SOL. On the other hand, the particle *outflux* of charge-exchange (CX) neutrals as measured by the classical charge-exchange analyzer for low particle energies by the LENA time-of-flight spectrometer shows the same isotopic scaling, i.e. larger fluxes and hence larger neutral pressures in hydrogen compared with deuterium discharges. In absolute numbers, Ohmic standard discharges with boronized walls show 1.6×10^{19} m^{-2} s^{-1} for hydrogen filling and 1.0×10^{19} m^{-2} s^{-1} for deuterium filling; the corresponding mean energy of the CX particles is measured to be 165 eV in the case of hydrogen and 332 eV in the case of deuterium [66].

From these data, the global particle confinement time τ_p of a deuterium plasma is found to exceed the value τ_p of a hydrogen plasma by 100 per cent. Exactly the same enhancement

$$\tau_p \propto A_i$$

is observed in, for example, TEXT [65], TEXTOR [42], and JET [31]. An interesting point is also the density dependence of τ_p for the hydrogen isotopes, as shown in

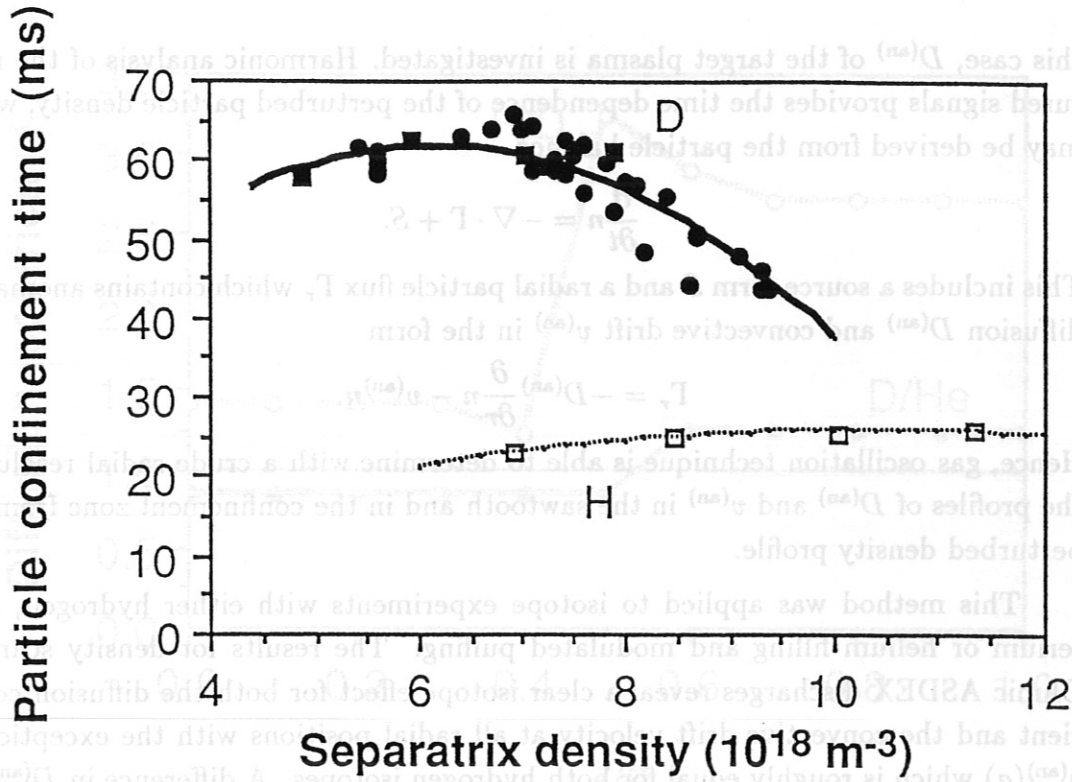

Figure 16: Particle confinement time as a function of the electron density at the separatrix.

Figure 16. With small separatrix density n_{es}, which means low recycling, τ_p increases with n_{es}. When the density is raised more and more, the plasma becomes impervious to neutrals and the recycling is limited to the very edge; accordingly, τ_p drops for high n_{es}. In between, τ_p reaches its maximum value at an optimum separatrix density. Figure 16 reveals that this principal relationship $\tau_p(n_{es})$ is fulfilled for both hydrogen and deuterium, but the absolute numbers of τ_p are much higher for deuterium than for hydrogen and the optimum n_{es} is shifted towards a smaller value for deuterium compared with hydrogen. As a remark, we refer to the Improved Ohmic Confinement in ASDEX where a similar dependence of τ_p on n_{es} was discovered [67].

Particle transport studies in the bulk plasma of ASDEX were performed experimentally with the help of neon-seeded pellets [59] or sinusoidally modulated gas puffing [68]. The first method evaluates the diffusion coefficients of neon to be $D^{(an)} \approx 0.4$ m^2/s for deuterium and $D^{(an)} \approx 0.6$ m^2/s for hydrogen background plasmas with Ohmic heating. Thus, the diffusion coefficient of impurities in its dependence on the mass of the background plasma is studied. The second method induces small density perturbations around the equilibrium value which can be followed by the different radial channels of the ASDEX HCN-laser interferometer. In

this case, $D^{(an)}$ of the target plasma is investigated. Harmonic analysis of the measured signals provides the time dependence of the perturbed particle density, which may be derived from the particle balance

$$\frac{\partial}{\partial t} n = -\nabla \cdot \Gamma + S.$$

This includes a source term S and a radial particle flux Γ_r which contains anomalous diffusion $D^{(an)}$ and convective drift $v^{(an)}$ in the form

$$\Gamma_r = -D^{(an)} \frac{\partial}{\partial r} n - v^{(an)} n.$$

Hence, gas oscillation technique is able to determine with a crude radial resolution the profiles of $D^{(an)}$ and $v^{(an)}$ in the sawtooth and in the confinement zone from the perturbed density profile.

This method was applied to isotope experiments with either hydrogen, deuterium or helium filling and modulated puffing. The results for density scans in Ohmic ASDEX discharges reveal a clear isotope effect for both the diffusion coefficient and the convective drift velocity at all radial positions with the exception of $v^{(an)}(a)$ which is roughly equal for both hydrogen isotopes. A difference in $D^{(an)}$ for both radial ranges is observed already in the LOC regime; the difference is largest in the SOC regime. Figure 17 shows the ratios of hydrogen to deuterium and deuterium to helium data for $D^{(an)}$ and $v^{(an)}$ in two series of Ohmic ASDEX discharges. The comparison between hydrogen and deuterium was performed with carbonized walls and $\overline{n}_e = 3 \times 10^{19}$ m^{-3}, $I_p = 320$ kA, $B_t = 2.2$ T, $q_a = 3.3$; the comparison between deuterium and helium was performed with boronized walls and $\overline{n}_e = 5 \times 10^{19}$ m^{-3}, $I_p = 320$ kA, $B_t = 2.2$ T, $q_a = 3.3$. The observations of different transport coefficients agree well with the finding that particle confinement for deuterium is superior to that for hydrogen (see Section 11). Quantitatively, the diffusion coefficient starts roughly as $D^{(an)} \propto A_i^{-1/2}$ for low densities and as $D^{(an)} \propto A_i^{-1}$ for the highest densities. The L-mode of high-density, neutral-beam-heated plasmas ($P_{NI} \leq 1.4$ MW) shows a scaling $D^{(an)} \propto A_i^{-1}$ similar to that of the Ohmic case, but an appreciably larger inward convection in the confinement region for deuterium than for hydrogen (see Figure 18); this leads to even better particle confinement in L-mode deuterium discharges.

The diffusion coefficient $D_s^{(an)}$ in the *SOL* plasma has been derived from the usual simple SOL model to be

$$D_s^{(an)} = \lambda_n^2 v_{\|} / L_c.$$

Inserting the measured separatrix data, we see a clear isotope effect, namely [69]

$$D_s^{(an)} \propto A_i^{-0.6}$$

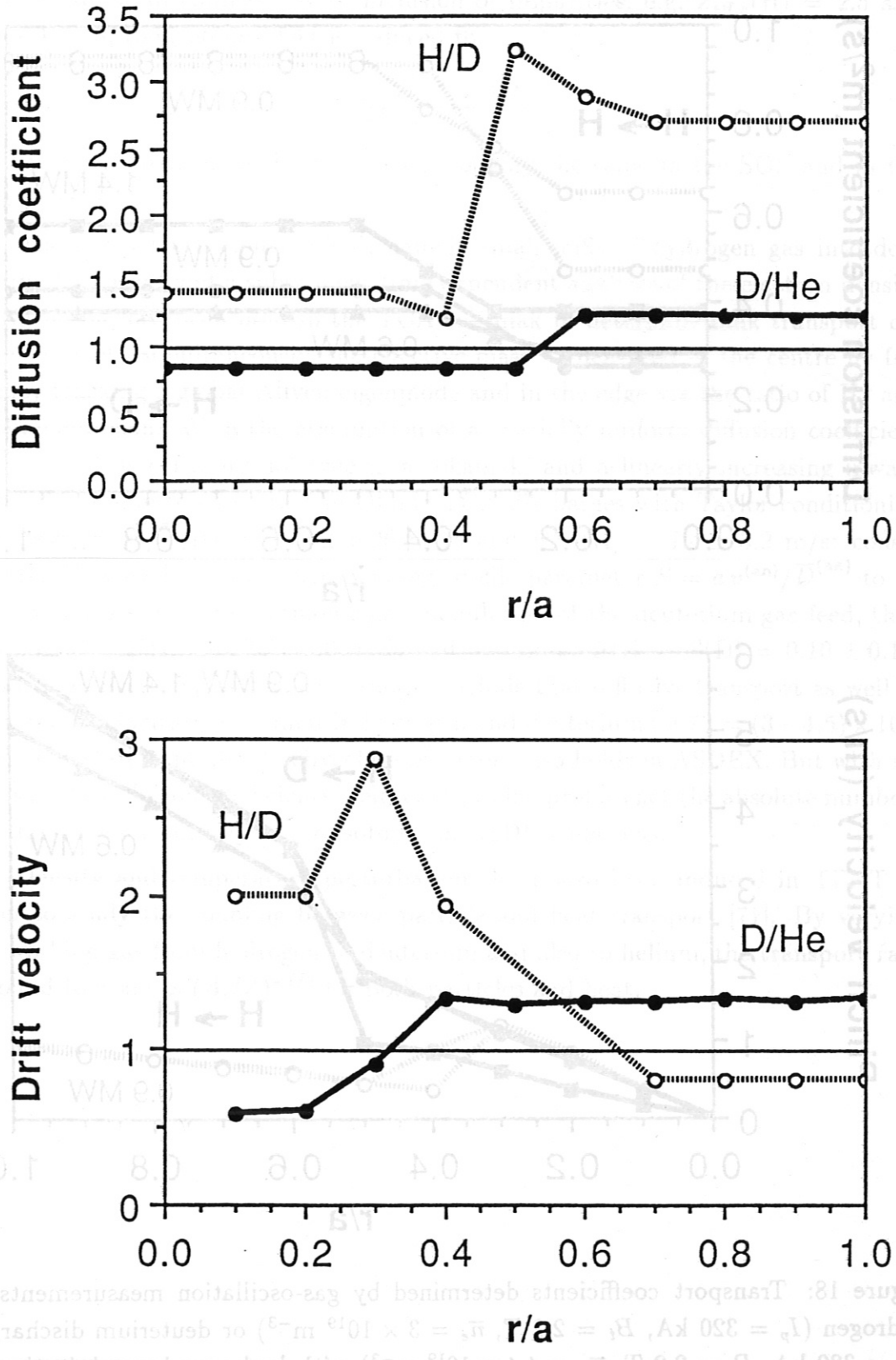

Figure 17: Ratio of transport coefficients determined by gas-oscillation measurements in Ohmic ASDEX discharges with hydrogen, deuterium or helium fuelling. (a) Diffusion coefficient and (b) inward drift velocity.

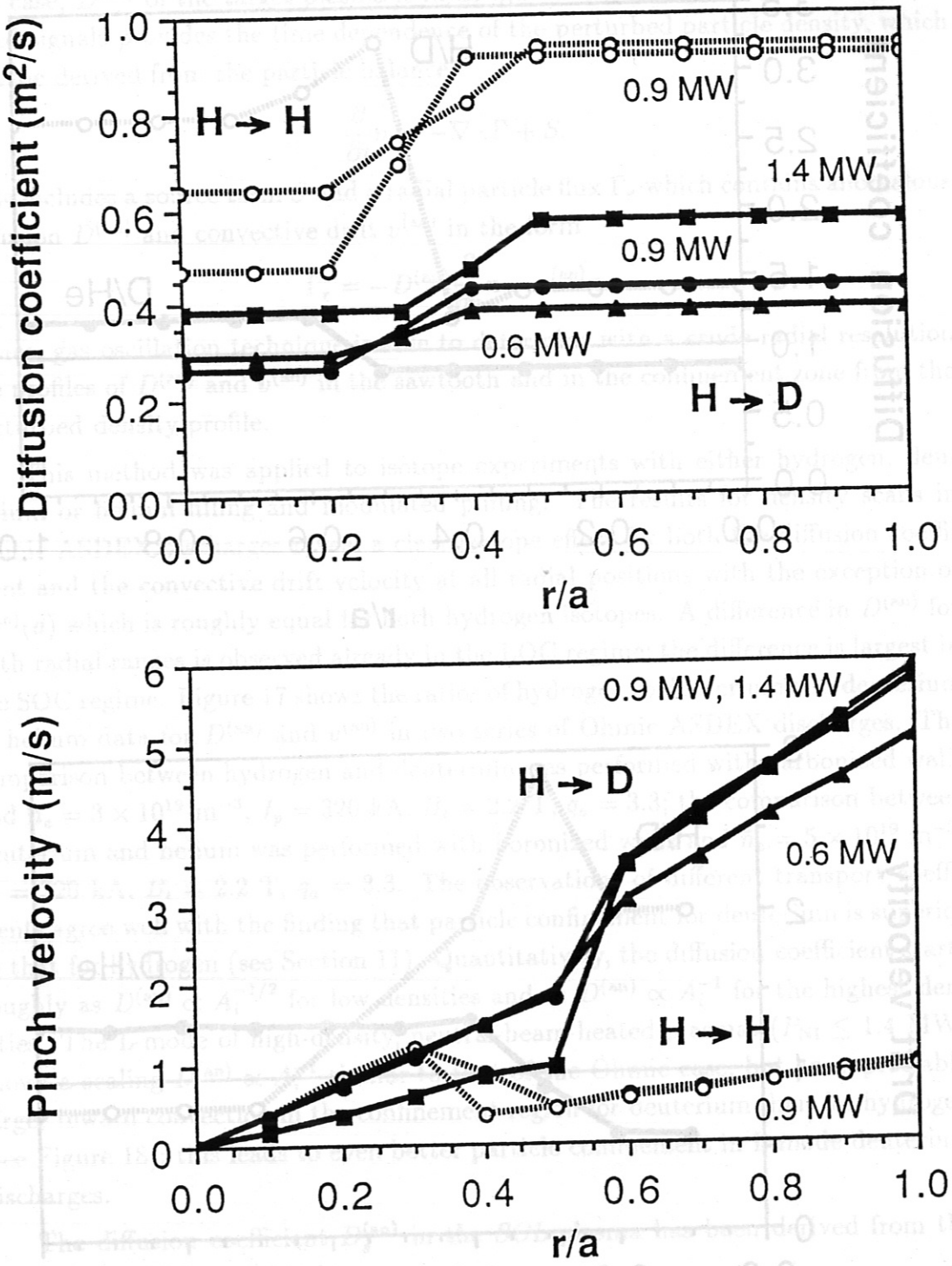

Figure 18: Transport coefficients determined by gas-oscillation measurements in hydrogen (I_p = 320 kA, B_t = 2.2 T, $\overline{n}_e = 3 \times 10^{19}$ m^{-3}) or deuterium discharges (I_p = 380 kA, B_t = 2.2 T, $\overline{n}_e = 4.4 \times 10^{19}$ m^{-3}) with hydrogen beam injection of P_{NI} = 0.6, 0.9, 1.4 MW.
(a) Diffusion coefficient and (b) inward drift velocity.

in pure Ohmic discharges. With inclusion of impurities, e.g. $Z_{\mathrm{eff},s}(\mathrm{H}) = 2.5$ and $Z_{\mathrm{eff},s}(\mathrm{D}) = 3$, the isotope effect is reduced to

$$D_s^{(\mathrm{an})} \propto A_i^{-0.37}.$$

In conclusion, anomalous diffusion scales roughly the same in the SOL and in the bulk plasma.

Another perturbation method, namely small puffs of hydrogen gas into deuterium discharges and a subsequent time-dependent analysis of the electron density perturbation, has been used in the TCA tokamak to determine bulk transport coefficients [70]. Simultaneously, the effective mass is measured in the centre by frequency tracking a global Alfvén eigenmode and in the edge via the ratio of H_β and D_β line emission. With the assumption of a spatially uniform diffusion coefficient $\overline{D}^{(\mathrm{an})}$, which is certainly not true in a tokamak, and a linearly increasing inward drift $v^{(\mathrm{an})}$, the authors extract in Ohmic TCA discharges with Taylor conditioning the averages $\overline{D}^{(\mathrm{an})}(\mathrm{H}) = 0.76 \pm 0.06$ m^2/s and $v^{(\mathrm{an})}(\mathrm{H}) = 7.4 \pm 3.2$ m/s; consequently, they evaluate the corresponding profile parameter $S = a\, v^{(\mathrm{an})}/\overline{D}^{(\mathrm{an})}$ to be $S(\mathrm{H}) = 1.7 \pm 0.6$. From harmonic gas modulation of the deuterium gas feed, they measure $D^{(\mathrm{an})}(\mathrm{D}) = 0.70 \pm 0.20$ m^2/s and determine $S(\mathrm{H}) - S(\mathrm{D}) = 0.10 \pm 0.15$. From these average results, the authors conclude that diffusive transport as well as convection velocities are similar in hydrogen and deuterium for $\overline{n}_e = (3-4.5) \times 10^{19}$ m^{-3}. The statement about convective transport also holds in ASDEX. But with respect to the diffusion coefficients, neither the radial profiles nor the absolute numbers are the same for both hydrogen isotopes in ASDEX plasmas.

Density and temperature perturbations have also been induced in TEXT in order to study the coupling between particle and heat transport [71]. By varying the working gas from hydrogen to deuterium and also to helium, the transport rate is found to scale as $(A_i/Z)^{-1/2}$ for both particles and heat.

13 Helium discharges

With respect to the underlying physical interpretation, it is necessary to distinguish between pure mass and specific mass effects of the isotope mix. Here, helium-fuelled discharges may help because they extend the investigations to $A_i = 4$ and simultaneously have the same $A_i/Z = 2$ as deuterium-fuelled plasmas. On the other hand, the atomic physics as well as the edge behaviour (e.g. recycling) is quite different for helium as compared to the hydrogen isotopes. Moreover, helium discharges are naturally characterized by a factor of 2 lower ion density due to $Z = 2$ and hence 25 % less charged particles compared with hydrogen plasmas. The same energy content thus needs much hotter particles.

The comparison of bulk parameters reveal striking similarities of helium and deuterium discharges on the one hand and hydrogen discharges on the other [74]: Radial density profiles look slightly more peaked in helium than in deuterium plasmas, whereas the volume-integrated radiation profiles is about the same, although Z_{eff} is different. The sawtooth repetition time takes roughly the same numbers, too. Density limit discharges in deuterium and helium differ in bulk density limit due to profile effects but can be described by a common edge density limit [15]. Since both transport parameters $D^{(\text{an})}$ and $v^{(\text{an})}$ in helium discharges resemble the deuterium values (see Figure 17), it is suggested that the isotope effect depends on the mass number per electron (A_i/Z) [75].

Ohmically heated TFTR plasmas also show no significant difference in the diffusion coefficient for deuterium or helium fuelling [76].

Detailed transport studies in TEXT, however, indicate that the diffusion coefficient is essentially the same in hydrogen and helium plasmas and the major difference is in the pinch velocity which is three times larger in helium than in hydrogen [65]. Doublet III-D experiments [27] seem to indicate that helium discharges have confinement comparable to that of hydrogen discharges, in other words that τ_E scales as A_i/Z^2.

14 Stability and boundary conditions

It is important to resolve whether the isotope mass *intrinsically* enters the diffusivities, i.e. $\chi_e, \chi_i = f(A_i)$, or whether the ion mass changes the *onset* conditions of an instability, i.e. $\chi_H = \chi_1 + \chi_2 > \chi_1 = \chi_D$. For the latter situation, the damping of ion temperature gradient (ITG) driven turbulence is studied. These η_i modes set in if the radial density profile exceeds a certain broadness in relation to the temperature profile, i.e. $\eta_i > \eta_{i,crit}$. In this context, it is an important general observation that radial density profiles in deuterium are always more peaked than in hydrogen.

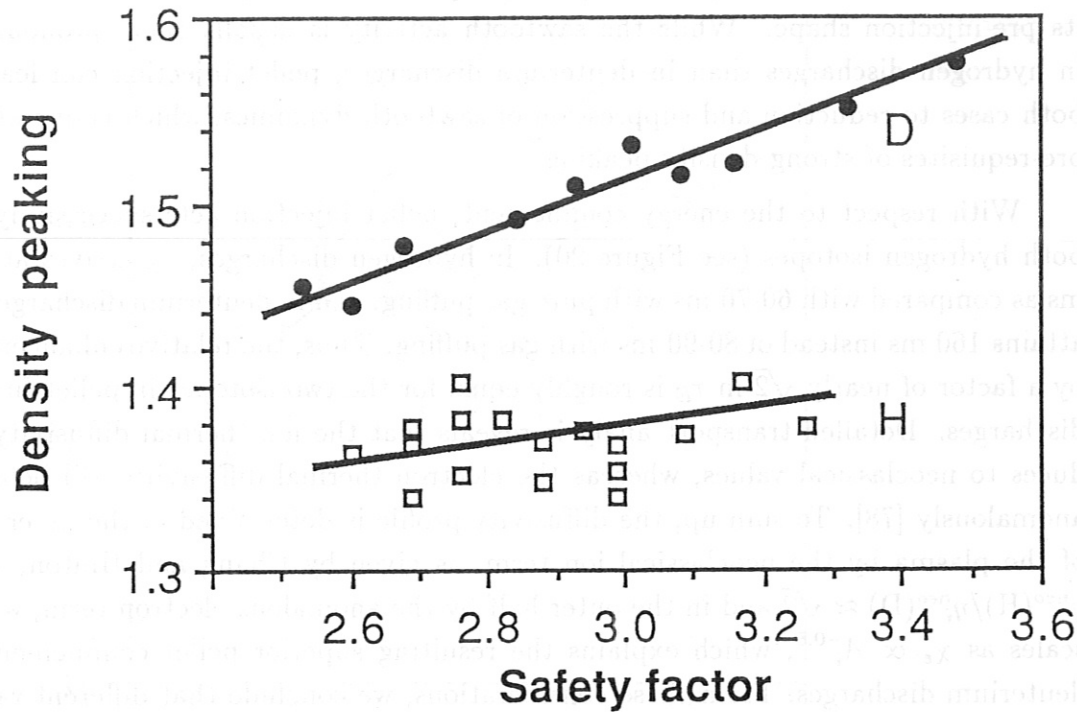

Figure 19: Central density peaking factor $n_{e0}/\langle n_e \rangle$ as a function of safety factor q_a for Ohmic ASDEX discharges with either hydrogen or deuterium fuelling.

Regression analysis yields

$$n_{e0}/\langle n_e \rangle \propto A_i^{\alpha}$$

with $0.17 \leq \alpha \leq 0.25$ (see Tables 1 and 2) and, as an example, Figure 19 shows the central density peaking factor $n_{e0}/\langle n_e \rangle$ as a function of safety factor q_a for Ohmic ASDEX discharges. In fact, tokamak plasmas with radially peaked density profiles show remarkably improved energy and particle confinement [77]. The strongest peaking is observed in pellet-fuelled discharges where sawteeth are efficiently suppressed and

bulk fuelling supplements edge fuelling. Therefore, transport investigations were performed for hydrogen pellet injection into hydrogen plasmas compared with deuterium pellet injection into deuterium plasmas. Both cases should have sufficiently peaked density profiles such that the critical threshold for ITG driven turbulence will not be exceeded.

For these studies, the centrifugal pellet injector in ASDEX was modified to inject hydrogen as well as deuterium pellets with 1.7×10^{20} atoms [78]. Both pellet types trigger strong peaking $n_{e0}/\langle n_e \rangle = 2.6$ of the radial density profile, although the pellets penetrate only up to $a/2$; this peaking can last over several confinement times. On the other hand, the temperature profile reverts on a fast time scale to its pre-injection shape. While the sawtooth activity is usually more pronounced in hydrogen discharges than in deuterium discharges, pellet injection can lead in both cases to reduction and suppression of sawtooth dynamics, which is one of the pre-requisites of strong density peaking.

With respect to the energy confinement, pellet injection acts successfully for both hydrogen isotopes (see Figure 20). In hydrogen discharges, τ_E arrives at 110 ms as compared with 60-70 ms with pure gas puffing, and in deuterium discharges τ_E attains 160 ms instead of 80-90 ms with gas puffing. Thus, the relative enhancement by a factor of nearly $\sqrt{2}$ in τ_E is roughly equal for the two isotopes in pellet-fuelled discharges. Detailed transport analysis reveals that the ion thermal diffusivity reduces to neoclassical values, whereas the electron thermal diffusivity still behaves anomalously [78]. To sum up, the diffusivity profile is determined in the inner half of the plasma by the neoclassical ion term, as given by Chang and Hinton, with $\eta_i^{neo}(\mathrm{H})/\eta_i^{neo}(\mathrm{D}) \approx \sqrt{2}$ and in the outer half by the anomalous electron term, which scales as $\chi_e \propto A_i^{-0.5}$, which explains the resulting superior pellet confinement of deuterium discharges. From these considerations, we conclude that different radial density profiles of hydrogen compared with deuterium are of minor importance in explaining the different energy confinement. In addition, we do not expect that the higher energy confinement of deuterium discharges is caused by density profile conditions which stabilize ITG driven turbulence whereas this mode contributes to the enhanced losses in hydrogen.

We now concentrate on the different temperature profiles of hydrogen compared to deuterium and determine the changes in the heat transport coefficients. This local transport analysis has been performed for high-density Ohmic plasmas ($B_t = 2.2$ T, $I_p = 420$ kA, $\overline{n}_e = 7.5 \times 10^{19}$ m^{-3}), where the different sawtooth activities of hydrogen and deuterium were separated out by a sawtooth model for the core plasma. In these discharges, the radial density profiles look similar for hydrogen and deuterium and both are characterized by $\eta_i > \eta_{i,crit}$. Figure 21 shows the corresponding results

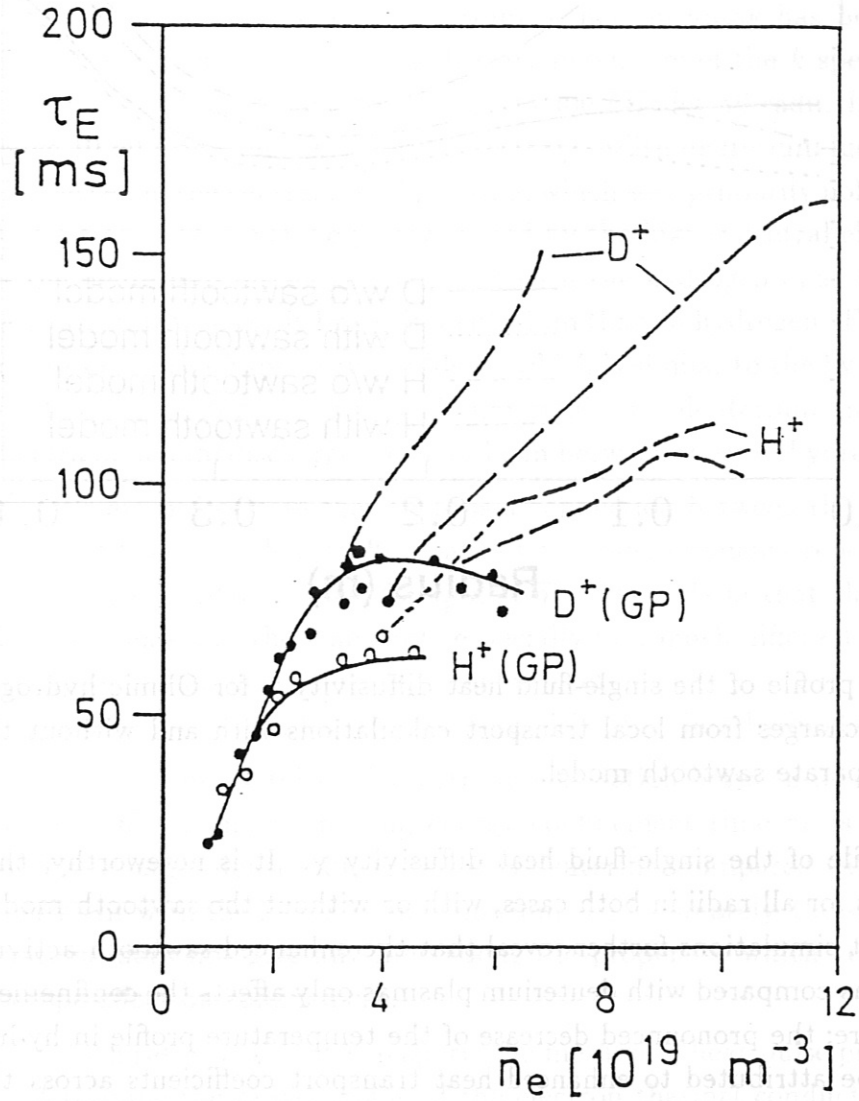

Figure 20: Energy confinement time as a function of electron density $\overline{n}_e$ for pellet injection cases compared with gas puffing (GP) [78].

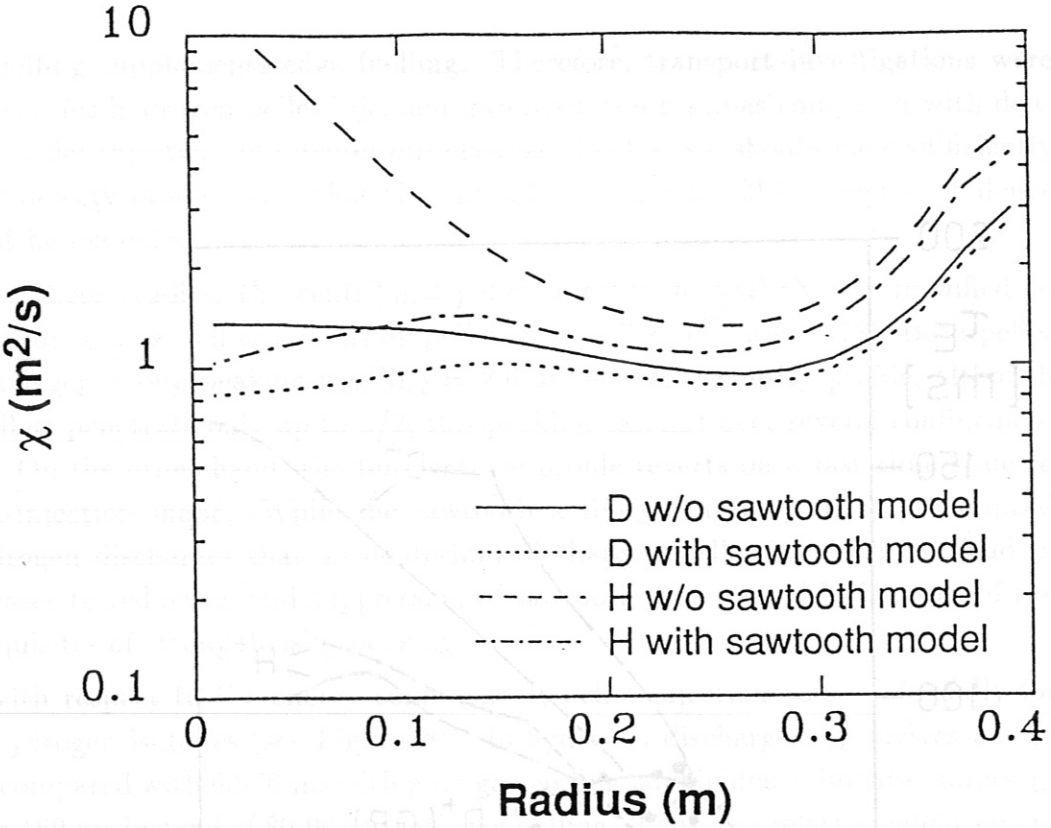

Figure 21: Radial profile of the single-fluid heat diffusivity χ for Ohmic hydrogen and deuterium discharges from local transport calculations with and without the application of a separate sawtooth model.

for the radial profile of the single-fluid heat diffusivity χ. It is noteworthy, that $\chi(\mathrm{D}) < \chi(\mathrm{H})$ holds for all radii in both cases, with or without the sawtooth model. The local transport simulations further reveal that the enhanced sawtooth activity of hydrogen plasmas compared with deuterium plasmas only affects the confinement in the plasma centre; the pronounced decrease of the temperature profile in hydrogen plasmas can be attributed to enhanced heat transport coefficients across the *entire* plasma cross section.

15 Fluctuations and transport

With the FIR collective laser scattering system, an isotope scan for the k spectra of Ohmic ASDEX discharges (B_t = 2.2 T, I_p = 320 kA, q_a = 3.3, $\overline{n}_e = 5.5 \times 10^{19}$ m^{-3}) with either hydrogen, deuterium or helium filling has been measured ([79]; [80]). With hydrogen fuelling, a distinct maximum of the k spectrum appears at a few cm^{-1} in the high-frequency range 35-400 kHz for all radii. In the low-frequency range 10-60 kHz, there is a continuous drop. With deuterium fuelling, no maximum is observed in the central radial position, which sees primarily poloidally propagating fluctuations. This may be partly caused by the higher central electron temperature in the deuterium discharge compared with the hydrogen one. Simultaneously, the total scattered power is larger in deuterium than in hydrogen. For the outer radii, a maximum in the k spectrum builds up which is similar to the hydrogen feature. The low-frequency range gives very similar results for deuterium and hydrogen. The k spectra of helium discharges seem to lie in between those of hydrogen and deuterium.

We are not certain that there is a connection between the global particle confinement time and density fluctuations but measurements reported by TEXT [65] always give similar scalings for τ_p and $\widetilde{n_e}$. They claim that the main isotopic dependence exists in the transport, especially in a much different convective velocity. Owing to the lower particle flux, the convective energy flux in a deuterium plasma also contributes much less to the energy loss than in a hydrogen plasma.

Since on many tokamaks a strong correlation between increasing density fluctuations $\widetilde{n_e}/n_e$ and decreasing energy confinement time τ_E is observed (e.g. [81]; [82]), the larger density fluctuations in deuterium compared with hydrogen are not consistent with the larger τ_E in deuterium. Unfortunately, the study of density fluctuations does not give any hint about the properties which could give rise to the isotope effect on confinement.

With respect to heat transport, the method of heat pulse propagation was used to determine the radial profile of the electron thermal conductivity χ_e ([83]; [84]). In Ohmic discharges ($\overline{n}_e = 2 \times 10^{19}$ m^{-3}, I_p = 320 kA, B_t = 2.2 T, q_a = 3.3), it is $\chi_e = 4 \pm 1$ m^2/s with either hydrogen or deuterium fuelling, i.e. no definite conclusions on the isotope dependence of χ_e can be drawn in ASDEX different from the single-fluid transport analysis. Similarly, measurements on TEXTOR [84], yield $\chi_e(a/2) \approx 3.0 \pm 0.3$ m^2/s in hydrogen plasmas ($\overline{n}_e = 2.0 \times 10^{19}$ m^{-3}) and $\chi_e(a/2) \approx 4.0 \pm 0.4$ m^2/s in deuterium plasmas ($\overline{n}_e = 1.4 \times 10^{19}$ m^{-3}), i.e. the large optical depth of about 1 in the boundary plasma of TEXTOR does not allow a definite conclusion on the isotope dependence of χ_e. The situation is more clear in FTU [85] where sawtooth propagation studies reveal strong isotope effects on χ_e.

16 Theoretical attempts

Theoretical attempts usually fail to predict the right isotope effect on transport and confinement, i.e. a degradation from hydrogen to deuterium. *Therefore, the isotope effect is an unsolved fundamental problem in tokamak transport theory.* Neoclassical theory predicts the heat diffusivity to behave as $\chi_i \propto A_i^{1/2}$. The model of ion pressure gradient modes, which successfully derives the improved confinement properties of radially peaked density profiles, proposes $\chi_i \propto A_i^{1/2}$ and $\chi_e \propto A_i^0$ for the heat transport and $D^{(an)} \propto A_i^0$ for the particle diffusion; i.e. the isotope dependence comes along with the wrong sign (see also Section 14). Theories including resistivity via either resistive gradient modes or resistive ballooning modes also fail; they predict $\chi_e \propto A_i^0$ and $\chi_e \propto A_i^{1/2}$, respectively. It is worthwhile noting that theoretical attempts are mostly not able, too, to explain the correct isotope effect on momentum transport, especially on τ_Φ [86].

Recently, it was shown by two authors independently ([87]; [88]) that the introduction of a second ion species of different mass, namely an impurity ion, makes A_i an explicit parameter in the ITG mode turbulence. In fact, Coppi [87] derives a scaling formula for the energy confinement time $\tau_E \propto (A_i/Z_{\text{eff}})^{2/5}$ which agrees with the experimental observations in ASDEX, including helium discharges (see Section 13). Coppi [89] also suggested that the window of instability for impurity modes is broadened, when the main species is changed from deuterium to hydrogen, thus allowing for larger radial transport and leading to lower confinement. However, the simulations by Dominguez [88] are restricted to low Z_{eff}, i.e. high density. This quasi-linear analysis has also been extended from hydrogen to helium discharges. The results indicate a scaling $\tau_E \propto A_i^{0.56}/Z$ which is adapted to Doublet III-D but in contradiction to ASDEX observations.

Nevertheless, models based on *collisional* drift-wave turbulence in the *shear* region seem to yield the right answer, i.e. $\tau_E \propto (A_i/Z)^{0.5}$. An isotope mass scaling with a trend similar to this one is a natural result of any turbulence system whose maintenance depends on nonadiabatic electron dynamics. With a nonadiabatic, non-negligible temperature, it is implied that there are fluctuations as well as departures from the Boltzmann relation, $\tilde{n}/n = e\tilde{\phi}/T$. These effects arise from competition between turbulence in the presence of a gradient, which enhances them, and parallel dissipation mechanisms (e.g. collisional dissipation), which suppress them. The latter localize electron nonadiabaticity to a finite region about each resonant surface, for each (m, n) component. Taking collisional electrons as an example, the width to which they are localized can be expressed as

$$\Delta_D \sim (\omega_t \nu_e) L_s / k_y v_e,$$

where $k_y = m/r$, $L_s = qR/\hat{s}$, ω_t is the dynamic rate of the turbulence (scaling as $\omega_\star$ for the long-wavelength component), and v_e is the electron thermal velocity (here and below, the collisionless regime substitutes electron Landau damping and ω_t for the mechanism and dynamic rate of the dissipation, respectively, leaving electron/ion considerations unchanged). The layer of this size centred on each resonant surface is each mode's hydrodynamic layer (so named because of the character of the dynamics therein). For linear modes, these layers had always been believed negligible since for any roughly isotropic fluctuation (mode width Δ comparable to wavelength k_y^{-1}), the type believed to contribute most to the turbulent transport, the parallel dissipation, easily overpowers ω_t. However, in the case of electron drift-wave turbulence it has been shown that the characteristic Δ_D's of the turbulence are much wider at short wavelength than the linear counterparts, and that the nonadiabatic dynamics therein has the dominant role to play in the self-sustainment of the turbulence.

The importance of this for the isotope effect is that these hydrodynamic layer widths are determined solely by the electron dynamics itself: nowhere in the above equation does the ion mass enter. The effect of increasing the ion mass is indirect. In cases in which nonadiabatic electron dynamics controlls the turbulent energetics, increasing the ion mass simply increases the amount of plasma that must be moved by the same (unchanged) amount containing the nonadiabatic dynamics, for Δ_D is the width only of the nonadiabatic part, not the whole. The overall width is determined by ion physics: the interplay between perpendicular and parallel inertial motion (not necessarily involving "sheardamping"). The relative importance of the energy-trapping nonadiabatic electron part to the whole can be characterized by a parameter (again for the collisional example),

$$C \equiv \frac{\Delta_D^2}{\rho_s^2} \sim \frac{\nu_e}{\omega_t} \frac{m_e}{m_i} \frac{L_s^2}{L_n^2}.$$

Electron drift-wave turbulence in particular and a nonadiabatic electron-mediated contribution to other turbulent mechanisms in general have their strength roughly measured by this parameter. Full computations at two different values of C appear in [10] and confirm the point: increasing the ion mass lowers C while leaving the nominal nonadiabatic electron component's mode widths unchanged, with the result of lower turbulent amplitude, weaker average "phase angles" between $\tilde{n}$ and $\tilde{T}$ and $\tilde{\phi}$, and hence weaker transport of both energy and particles. An important point is that the turbulence does not affect transport diffusively, so that the attendant increase of the *ion* mode width (of $\tilde{\phi}$) has no direct effect. It is to be emphasized that the relevance of this carries over into the full, multi-resonant surface ("three-dimensional") situation. The localization in the slab case is controlled by the long-wavelength component, whose mode widths are sufficiently narrow (i.e. they are

sufficiently anisotropic) that the shear effects which influence it in the slab case should also do so in the multi-surface case. (This is also why the long-wavelength k_y is to be used in the above estimates, *not* the short-wavelength one.)

Speculating on the scaling [10], one may assume that the relative phases and amplitudes between the quantities $e\tilde{\phi}/T$, $\tilde{n}/n$, and $\tilde{T}/T$ have weaker dependences on parameters than the basic turbulence scales themselves. With the amplitudes roughly scaling as, for example, $\tilde{n}/n \sim \Delta_D/L_n$, a naïve estimate for the flux would be $q_T = \langle \frac{3}{2} n T v_x \rangle$, averaged over a flux surface, or, with nominal parameters of Δ_D/L_n for the amplitudes,

$$q_T \sim \frac{3}{2} n T c_s \frac{\Delta_D^2}{L^2},$$

where L is an overall scale length (for some combination of n and T). Only c_s has m_i-dependence, so that even in the case that toroidicity and profile dynamics change the electron scales, changing m_i/Z only should yield a confinement scaling of roughly $\tau_E \propto (m_i/Z)^{1/2}$. Note that any model situation in which non-adiabatic electron dynamics is important should exhibit the isotope effect in this way: the non-adiabatic part of the system has its role diminished whenever m_i/Z is increased.

One would expect the isotope effect to be strongest in regimes where the electron channel is dominant in the transport. In collisionless regimes, both trapped and circulating electrons have roles to play, and the trapped part may be less sensitive to these considerations (in the conventional view: this has *not* been substantiated by calculations which do not take it as an assumption). If the ion channel is the stronger, then the extent of the isotope effect should be limited to that to which the nonadiabatic electrons help drive the turbulence (the "mode" will be necessarily some sort of "ion mixing mode", since the selfsame $\tilde{\phi}$ is driven by both temperature gradients as well as the density one). If this becomes negligible, then the isotope effect in the present picture should vanish. This may explain the results from Doublet III-D that no isotope effect is observed in their L-mode phase (in which ion-temperature dynamics is widely believed to dominate).

A quite different theoretical approach follows the neutral particles in the *edge* plasma and their effects on plasma transport and rotation [90]. Indeed, analytical calculations of the neutral-plasma interactions, which take charge-exchange and impact ionization into account, give a thermal conductivity χ_n of neutral CX particles that scales as $\chi_n \propto A_i^{-0.5}$. In the TEXT edge region, χ_n and local τ_E are inversely related and hence $\tau_E \propto A_i^{0.5}$ holds there. Nevertheless, the significance of this local agreement, with regard to global confinement, remains to be investigated.

In order to derive general confinement scalings which combine edge *and* bulk phenomena, a multiple mechanism approach has also been suggested [91]. The

confinement zone is thought to be controlled by trapped electron (DTE) modes [92] and the edge region to be dominated by rippling modes and resistive ballooning modes. There, the difference in the neutral mean free paths between hydrogen and deuterium (see Section 10) plays an important role by modifying the profiles. As a result for Ohmic plasmas, the scaling formula

$$\tau_E \propto \langle n_e \rangle \times a^{2.3} \times R^{0.67} \times B_t^0 \times q_a^{0.33} \times A_i^{0.25}$$

is derived which has roughly the experimentally observed mass dependence. Moreover, the effect weakens slightly from $A_i^{0.33}$ to $A_i^{0.2}$ when the minor radius is raised from 0.5 to 1.0 m in consistence with the weaker isotope scaling on the larger tokamaks. For L-mode plasmas, the A_i dependence of τ_E is weakened or becomes even negative. For example, the confinement with rippling, DTE and resistive ballooning modes gives $\tau_E \propto A_i^{-0.10}$. Thus, while neutral penetration may be a contributing factor, it is not the main source of the observed superiority of deuterium fuelling.

17 Summary and Conclusions

From the above results, it can be concluded that the isotope mass is a substantial and robust parameter in tokamak confinement. Under *Ohmic* conditions, ASDEX and many other tokamaks show $\tau_E \propto A_i^{0.5}$ which was not expected by theory. Both collisional and turbulent transport theory predict that the plasma species with smaller gyro radius has the lower transport. Because of this fundamental discrepancy, we have studied in great detail isotopic dependences in particle, energy and momentum confinement and in the repetition time of sawteeth and ELMs during all experimental phases of ASDEX. Many tokamak experiments have noted the isotope effect and have thereby documented that the isotope mass is a fundamental scaling parameter. Furthermore, both the electron and the ion channels are influenced. In otherwise identical discharges, the electron temperature is larger in deuterium than in hydrogen over the whole cross-section. From electron transport-dominated LOC data with low $\overline{n}_e$ and high Z_{eff} up to ion transport-dominated SOC data with high $\overline{n}_e$ and $Z_{\text{eff}} \approx 1$, deuterium plasmas yield longer confinement times. The clean plasma conditions point to the fact that the isotope effect is not introduced by impurities and impurity collisions. Besides energy confinement, particle confinement $\tau_p \propto A_i^1$ as well as momentum confinement $\tau_\Phi \propto A_i^1$ are superior in ASDEX deuterium discharges. The pronounced isotope effects in the edge may be understood as a consequence of different energy fluxes into the scrape-off layer. Transport analysis for particles and energy reveal reduced values for $D^{(\text{an})}$ and $\chi^{(\text{an})}$ in deuterium plasmas over the whole cross-section. Moreover, the isotope effect shows up with strongly peaked density profiles in pellet refuelled discharges where ITG driven turbulence should be suppressed for both hydrogen isotopes. This leads us to the conclusion that the isotope effect does not rely on any additional onset condition for turbulence in the hydrogen case. A comparative analysis of Ohmic deuterium and helium plasmas point to a scaling $\tau_E \propto (A_i/Z)^{0.5}$ in ASDEX.

Under *L-mode* conditions, the isotope effect on τ_E is weakened in ASDEX and many other tokamaks, and it nearly vanishes in Doublet III-D with neutral injection although $\tau_E \propto A_i^{0.5}$ holds with electron cyclotron resonance heating in Doublet III-D. It is not clear *why* the isotope effects weaken under L-mode conditions compared with Ohmic data. One hint may be hidden in the Ohmic heating cycle: Reduced transport results in increased electron temperature and consequently in reduced input power which eventually improves energy confinement. In this case, the intrinsic A_i scaling would be weaker and more like $\tau_E \propto A_i^{0.33}$. Another possibility is that the isotope effect disappears in a fully turbulent medium because the scaling length is not determined any more by the gyro radius.

We support this conjecture with the remark that the isotope effect shows up clearly again under *H-mode* conditions. This has been taken into account in the recent ITER H-mode scaling.

Acknowledgements

The isotope effect was studied on ASDEX over a long period. The authors appreciate the support of the entire ASDEX Team during that time. We would like to thank the various operation teams on ASDEX for their hard, patient and devoted work. The reliable operation of ASDEX goes to their credit.

Thanks are also due to those who have contributed world-wide to fill Table 3.

Moreover, we would like to thank K. Lackner for carefully reading the manuscript and for valuable comments.

References

[1] WAGNER, F., BECKER, G., BEHRINGER, K., CAMPBELL, D., EBERHAGEN, A., et al., Phys. Rev. Lett. **49** (1982) 1408.

[2] SÖLDNER, F. X., MÜLLER, E. R., WAGNER, F., BOSCH, H. S., EBERHAGEN, A., et al., Phys. Rev. Lett. **61** (1988) 1105.

[3] STROTH, U., FUSSMANN, G., KRIEGER, K., MERTENS, V., WAGNER, F., BESSENRODT-WEBERPALS, M., et al., Nucl. Fusion **31** (1991) 2291.

[4] HUGILL, J. and SHEFFIELD, J., Nucl. Fusion **18** (1978) 15.

[5] PFEIFFER, W. and WALTZ, R. E., Nucl. Fusion **19** (1979) 51.

[6] GOLDSTON, R. J., Plasma Phys. Contr. Fusion **26** (1984) 87.

[7] KAYE, S. M., Phys. Fluids **28** (1985) 2327.

[8] KAYE, S. M., Survey of energy confinement scaling expressions, presented at ITER Specialists Meeting on Energy Confinement, Garching, 1988.

[9] YUSHMANOV, P. N., TAKIZUKA, T., RIEDEL, K. S., KARDAUN, O. J. W. F., CORDEY, J. G., KAYE, S. M., and POST, D. E., Nucl. Fusion **30** (1990) 1999.

[10] SCOTT, B. D., Phys. Fluids **B4** (1992) 2468.

[11] MÜLLER, E. R., BEHRINGER, K., and NIEDERMEYER, H., Nucl. Fusion **22** (1982) 1651.

[12] SCHNEIDER, U., POSCHENRIEDER, W., FUSSMANN, G., HOFMANN, J., KALLENBACH, A., et al., J. Nucl. Mater. **176-177** (1991) 350.

[13] RÖHR, H., STEUER, K.-H., and ASDEX-TEAM, Rev. Sci. Instrum. **59** (1988) 1875.

[14] STEUER, K.-H., RÖHR, H., and KURZAN, B., Rev. Sci. Instrum. **61** (1990) 3084.

[15] STÄBLER, A., MCCORMICK, K., MERTENS, V., MÜLLER, E. R., NEUHAUSER, J., et al., Nucl. Fusion **32** (1992) 1557.

[16] ISLER, R. C., KASAI, S., MURRAY, L. E., SALTMARSH, M., and MURAKAMI, M., Phys. Rev. Lett. **47** (1981) 333.

[17] MARMAR, E. S., RICE, J. E., and ALLEN, S. L., Phys. Rev. Lett. **45** (1980) 2025.

[18] BESSENRODT-WEBERPALS, M., MCCORMICK, K., SÖLDNER, F. X., WAGNER, F., BOSCH, H. S., et al., Nucl. Fusion **31** (1991) 155.

[19] MURMANN, H., WAGNER, F., ASDEX-TEAM, NI-TEAM, and ICRH-TEAM, Europhys. Conf. Abstr. **12B** (1988) 3.

[20] NOTERDAEME, J.-M., RYTER, F., WESNER, F., BOMBA, B., BOSCH, H.-S., et al., Nucl. Fusion Suppl. **1** (1989) 583.

[21] RYTER, F., STROTH, U., BRAMBILLA, M., ICRH-TEAM, ASDEX-TEAM, and NI-TEAM, Europhys. Conf. Abstr. **15C/III** (1991) 413.

[22] SÖLDNER, F. X., LEUTERER, F., BRAMBILLA, M., BÜCHSE, R., FAHRBACH, H.-U., et al., Nucl. Fusion Suppl. **1** (1991) 613.

[23] BESSENRODT-WEBERPALS, M., SÖLDNER, F., MÜLLER, E., MURMANN, H. D., POSCHENRIEDER, W., et al., Plasma Phys. Controlled Fusion **34** (1992) 443.

[24] GEHRE, O., GRUBER, O., MURMANN, H. D., ROBERTS, D. E., WAGNER, F., et al., Phys. Rev. Lett. **60** (1988) 1502.

[25] FUSSMANN, G., GRUBER, O., MÜLLER, E. R., NIEDERMEYER, H., et al., Plasma Phys. Contr. Nucl. Fusion Res. **1** (1988) 145.

[26] ASDEX-TEAM, Nucl. Fusion **29** (1989) 1959.

[27] SCHISSEL, D. P., BURRELL, K. H., DEBOO, J. C., GROEBNER, R. J., KELLMAN, A. G., et al., Nucl. Fusion **29** (1989) 185.

[28] MCGUIRE, K. and ROBINSON, D. C., Nucl. Fusion **19** (1979) 505.

[29] VLAD, G., BRACCO, G., and BURATTI, P., Nucl. Fusion **31** (1991) 1536.

[30] STÄBLER, A., WAGNER, F., BECKER, G., BERNHARDI, K., DITTE, U., et al., Energy confinement scaling of ASDEX L- and H-discharges, in *Proc. 4th Int. Symp. Heating in Toroidal Devices*, pages 3–19, Roma, 1984.

[31] TIBONE, F., BALET, B., BURES, M., CORDEY, J. G., JONES, T. C. C., et al., Europhys. Conf. Abstr. **16C/I** (1992) 19.

[32] ZOHM, H., WAGNER, F., ENDLER, M., GERNHARDT, J., HOLZHAUER, E., et al., Nucl. Fusion **32** (1992) 489.

[33] VOLLMER, O., RYTER, F., STEUER, K.-H., WAGNER, F., ZOHM, H., ASDEX-TEAM, and NI-TEAM, Europhys. Conf. Abstr. **15C/Part I** (1991) 385.

[34] STAMBAUGH, R., ALLEN, S., BRAMSON, G., BROOKS, N., BURRELL, K. H., et al., Plasma Phys. Controlled Fusion **30** (1988) 1585.

[35] BURRELL, K. H., ALLEN, S. L., BRAMSON, G., BROOKS, N. H., CARLSTROM, T. N., et al., Plasma Phys. Controlled Fusion **31** (1989) 1649.

[36] STALLARD, B. W., CONTENT, D. A., GROEBNER, R. J., HILL, D. N., JAMES, R., et al., Nucl. Fusion **30** (1990) 2235.

[37] ALLADIO, F., APRUZZESE, G., BARBATO, E., BARDOTTI, G., BARTIROMO, R., et al., Nucl. Fusion Suppl. **1** (1991) 153.

[38] ALLADIO, F., BERTON, F., BRACCO, G., BURATTI, P., TUDISCO, O., et al., Europhys. Conf. Abstr. **16C/I** (1992) 23.

[39] BARTLETT, D. V., BICKERTON, R. J., BRUSATI, M., CAMPBELL, D. J., CHRISTIANSEN, J. P., et al., Nucl. Fusion **28** (1988) 73.

[40] JET-TEAM – presented by CORDEY, J. G., The transport of energy and particles in JET plasmas, in *Proc. 14th IAEA Int. Conf. Plasma Phys. Controlled Nuclear Fusion Research*, Würzburg, 1992, IAEA-CN-56/D-3-4.

[41] KIKUCHI, M., SHIRAI, H., TAKIZUKA, T., KAMADA, Y., KOIDE, Y., et al., H-mode and L-mode confinement in JT-60 U, in *Proc. 14th IAEA Int. Conf. Plasma Phys. Controlled Nuclear Fusion Research*, Würzburg, 1992, IAEA-CN-56/A-3-3.

[42] SAMM, U., BOGEN, P., HARTWIG, H., HINTZ, E., HÖTHKER, K., et al., Europhys. Conf. Abstr. **13B** (1989) 995.

[43] BARNSLEY, C. W., SCOTT, S. D., BELL, M. G., BELL, R., BUDNY, R. V., et al., Energy confinement analysis of hydrogen isotope experiments on TFTR, Preprint, 1992.

[44] BESSENRODT-WEBERPALS, M., MCCORMICK, K., WAGNER, F., , and ASDEX-TEAM, J. Nucl. Mater. **176 & 177** (1991) 538.

[45] SCOTT, S. D., BARNES, C. W., et al., Preliminary analysis of species scaling experiments in TFTR, in *Proc. 32nd Annual Meeting APS-DPP*, 1990.

[46] ONGENA, J., CONRADS, H., MESSIAEN, A. M., VAN MASSENHOWE, G., WEYNANTS, R. R., et al., Overview of heating and improved confinement I-mode on TEXTOR with NBI and ICRH, in *Proc. 14th IAEA Int. Conf. Plasma Phys. Controlled Nuclear Fusion Research*, Würzburg, 1992, IAEA-CN-56/E-3-4.

[47] H-MODE DATABASE WORKING GROUP – presented by KARDAUN, O. J. W. F., ITER: Analysis of the H-mode confinement and threshold databases, in *Proc. 14th IAEA Int. Conf. Plasma Phys. Controlled Nuclear Fusion Research*, Würzburg, 1992, IAEA-CN-56/F-1-3.

[48] WAGNER, F. and STROTH, U., Plasma Phys. Controlled Fusion (manuscript, 1992).

[49] MURAKAMI, M., ACETO, S. C., ANABITARTE, E., ANDERSON, D. T., ANDERSON, F. S. B., et al., Nucl. Fusion Suppl. **2** (1991) 455.

[50] NEUHAUSER, J., BESSENRODT-WEBERPALS, M., BRAAMS, B. J., CARLSON, A., CHODURA, R., et al., Plasma Phys. Controlled Fusion **31** (1989) 1551.

[51] MCCORMICK, K., BESSENRODT-WEBERPALS, M., MÜLLER, E. R., NEUHAUSER, J., NIEDERMEYER, H., et al., J. Nucl. Mater. **176-177** (1991) 89.

[52] SAMM, U., BOGEN, P., BORA, D., CLAASSEN, H. A., GERHAUSER, H., et al., J. Nucl. Mater. **176-177** (1991) 273.

[53] SCHORN, R. P., WOLFRUM, E., AUMAYR, F., HINTZ, E., RUSBÜLDT, D., and WINTER, H., Nucl. Fusion **32** (1992) 351.

[54] MCCORMICK, K., PIETRZYK, Z. A., MURMANN, H., LENOCI, M., and ASDEX-TEAM, J. Nucl. Mater. **145-147** (1987) 215.

[55] TENDLER, M. B. and ÅGREN, O., Phys. Fluids **25** (1982) 1037.

[56] NIEDERMEYER, H., BECKER, G., BOMBA, B., BRUHNS, H., BÜCHL, K., et al., Plasma Phys. Controlled Fusion **30** (1988) 1443.

[57] HAAS, G., POSCHENRIEDER, W., NEUHAUSER, J., KAESDORF, S., ASDEX-TEAM, and NI-TEAM, J. Nucl. Mater. **162-164** (1989) 509.

[58] ROTH, J. and JANESCHITZ, G., Nucl. Fusion **29** (1989) 915.

[59] BEHRINGER, K., FUSSMANN, G., POSCHENRIEDER, W., TAGLAUER, E., BERNHARDI, K., et al., Europhys. Conf. Abstr. **7D** (1983) 467.

[60] ALI MAHDAVI, M., DEBOO, J. C., HSIEH, C. L., OHYABU, N., STAMBAUGH, R. D., and WESLEY, J. C., Phys. Rev. Lett. **47** (1981) 1602.

[61] KEILHACKER, M., LACKNER, K., BEHRINGER, K., MURMANN, H., and NIEDERMEYER, H., Phys. Scripta (1982) 443.

[62] HARRISON, M. F. A., HARBOUR, P. J., and HOTSTON, E. S., Nucl. Technol./Fusion **3** (1983) 432.

[63] STANGEBY, P. C., Phys. Fluids **27** (1984) 682.

[64] RITZ, C. P., BRAVENEC, R. V., SCHOCH, P. M., BENGTSON, R. D., BOEDO, J. A., et al., Phys. Rev. Lett. **62** (1989) 1844.

[65] ROWAN, W. L., MEIGS, A. G., AUSTIN, M. E., CHEN, J. Y., HICKOK, R. L., et al., Europhys. Conf. Abstr. **14B** (1990) 26.

[66] VERBEEK, H. and ASDEX-TEAM, Observations with the Low Energy Neutral Analyzer (LENA) on ASDEX. Part I: Ohmic discharges, Technical Report 9/84, IPP Garching, 1991.

[67] BESSENRODT-WEBERPALS, M., CARLSON, A., HAAS, G., MURMANN, H. D., NEUHAUSER, J., et al., Plasma Phys. Controlled Fusion **32** (1990) 21.

[68] GENTLE, K. W., GEHRE, O., and KRIEGER, K., Nucl. Fusion **32** (1992) 217.

[69] MCCORMICK, K., KYRIAKAKIS, G., NEUHAUSER, J., KAKOULIDIS, E., SCHWEINZER, J., and TSOIS, N., J. Nucl. Mater. (submitted, 1992).

[70] DUDOK DE WIT, T., DUVAL, B. P., JOYE, B., and LISTER, J. B., Nucl. Fusion **31** (1991) 359.

[71] BROWER, D. L., KIM, S. K., WENZEL, K. W., AUSTIN, M. E., FOSTER, M. S., et al., Phys. Rev. Lett. **65** (1990) 337.

[72] KALLENBACH, A., MAYER, H. M., FUSSMANN, G., MERTENS, V., STROTH, U., VOLLMER, O., and ASDEX-TEAM, Plasma Phys. Controlled Fusion **33** (1991) 595.

[73] BURRELL, K. H., GROEBNER, R. J., ST. JOHN, H., and SERAYDARAN, R. P., Nucl. Fusion **28** (1988) 3.

[74] BESSENRODT-WEBERPALS, M., GEHRE, O., HOFMANN, J., MURMANN, H., SILLER, G., and ASDEX-TEAM, J. Nucl. Mater. (submitted, 1992).

[75] GEHRE, O., GENTLE, K. W., ASDEX-TEAM, and NI-TEAM, Europhys. Conf. Abstr. **15C** (1991) I/97.

[76] STRATTON, B. C., FONCK, R. J., HULSE, R. A., RAMSEY, A. T., TIMBERLAKE, J., et al., Nucl. Fusion **29** (1989) 437.

[77] MERTENS, V., BESSENRODT-WEBERPALS, M., DODEL, G., GEHRE, O., GIANNONE, L., et al., Plasma Phys. Controlled Fusion **32** (1990) 965.

[78] GRUBER, O., KAUFMANN, M., LACKNER, K., LANG, R. S., MERTENS, V., et al., Europhys. Conf. Abstr. **12B** (1988) 27.

[79] DODEL, G., HOLZHAUER, E., GIANNONE, L., NIEDERMEYER, H., GERNHARDT, J., and ASDEX-TEAM, Europhys. Conf. Abstr. **14B** (1990) 207.

[80] HOLZHAUER, E. and DODEL, G., Rev. Sci. Instrum. **61** (1990) 2817.

[81] TFR Group and TRUC, A., Nucl. Fusion **26** (1986) 1303.

[82] CROWLEY, T. and MAZZUCATO, E., Nucl. Fusion **25** (1985) 507.

[83] GIANNONE, L., RIEDEL, K., STROTH, U., EBERHAGEN, A., GRUBER, O., MERTENS, V., and ASDEX-TEAM, Europhys. Conf. Abstr. **14B** (1990) I/191.

[84] GIANNONE, L., KRÄMER-FLECKEN, A., MERTENS, V., RIEDEL, K., WAGNER, F., and WAIDMANN, G., Europhys. Conf. Abstr. **15C** (1991) I/213.

[85] JACCHIA, A. et al., ? isotope experiments in FTU ?, Private communication, 1992.

[86] OSIPENKO, M. V., POGUTSE, O. P., and SHURYGIN, R. V., Nucl. Fusion Suppl. **2** (1989) 221.

[87] COPPI, B., Nucl. Fusion Suppl. **2** (1991) 413.

[88] DOMINGUEZ, R., Nucl. Fusion **31** (1991) 2063.

[89] COPPI, B., DETRAGIACHE, P., MIGLIUOLO, S., NASSI, M., ROGERS, B., et al., (1992), IAEA-CN-56/D-3-1(C).

[90] HAZELTINE, R. D., CALVIN, M. D., VALANJU, P. M., and SOLANO, E. R., Nucl. Fusion **32** (1992) 3.

[91] SHEFFIELD, J., Nucl. Fusion **29** (1989) 1347.

[92] ROGISTER, A., HASSELBERG, G., WAELBROECK, F., and WEILAND, J., Transport through dissipative trapped electron mode and toroidal ion temperature gradient mode in TEXTOR, Technical Report Jül–2173, KFA Jülich, 1987.